CARLETON UNIVERSITY
DEPARTMENT OF ELECTRONICS

Modeling and Design of a Frequency-Controlled Class-E Transcutaneous Energy Transfer System

by

Ahmad Mizannojehdehi

A Thesis Submitted
in Partial Fulfillment of the
Requirements for the Degree

MASTER OF APPLIED SCIENCE

Ottawa, Ontario

January, 2007

Your file Votre référence
ISBN: 978-0-494-23343-6
Our file Notre référence
ISBN: 978-0-494-23343-6

ABSTRACT

A transcutaneous energy transfer system is used to transfer energy through a human body's skin by using a pair of coupled coils, one of which is implanted under the skin and the other one placed over it at the exterior side of the body. Electromagnetic flux, produced by current driven to the external coil, transfers power through the skin to the secondary coil.

In this thesis a design methodology is proposed in which a Class-E amplifier is used to provide the driving current of the external coil and the output voltage is regulated by variation of the operation frequency of the system. The mathematical models of this system are developed, by which, for a particular application the design method is applied, the system is implemented and its simulation and experimental results are reported.

The results of this work indicate that this system can compensate the power transfer variation due to coupling, load and external battery voltage variation and, as such, employing a frequency-controlled Class-E technique is an effective way of controlling the transcutaneous stream of power for an implanted electronic device.

The developed system in this thesis demonstrates power transfer efficiency of 76% for a separation distance of 15 mm between the two coils and can tolerate a ± 5 mm separation variation between the coils for a fixed output voltage. These specifications could be even further improved through employment of better fabrication techniques and utilization of highest quality electronic parts.

Acknowledgments

I wish to thank my thesis supervisors, Dr. Maitham Shams for his warm welcome, support and advice; and Dr. Tofy Mussivand for opening my eyes to the world of biomedical and providing the opportunity of contribution to this world.

I thank my wife, Dr. Nasrin Hojjat, for her invaluable help and sharing of hard situation with me.

This thesis has been financially supported partly by NSERC and Medical Devices Center of the University of Ottawa Heart Institute which is highly appreciated.

Contents

List of Figures

Chapter 1

INTRODUCTION

Implanted electronic devices provide an improved quality of life for patients suffering from malfunctioning of an organ. Supplying of electric power for the electronic implanted devices is one of the most difficult issues in which many fields of electrical engineering are involved. In the early stages of development of artificial organs, percutaneous energy transfer method was used. In this method, electrical power is transferred via wires connecting the implanted device to plugs passed through pierced skin. This method inherently provides high risks of infections and medical complications for a recipient of the system. Furthermore the subject of the implanted device is limited to restricted living conditions and should be always under very rigorous clinical care to prevent any infection. Transcutaneous energy transfer or transferring power through the intact skin, which is addressed in this thesis, inherently doesn't have the infections problem therefore is a superior solution to the problem of powering up an implanted electronic device [1]-[5]. A transcutaneous energy transfer system uses a wireless link to transfer power through the intact skin. The recipient of this

system is not subjected to infections from the exterior of the body and can enjoy a less restricted and better quality of life with much less clinical care as compared to the case where percutaneous energy transfer system is used. Nonetheless, designing a transcutaneous energy transfer system is a challenging work. It should be highly efficient and reliable, not emit too much heat to overheat the surrounding tissues where it is implanted, and should always have a stable working condition. Any progress in development of the transcutaneous energy transfer system technology has a vital influence in the development of implanted electronic devices and artificial organs and any contribution to this technology has direct effect on better living and the quality of life of the human beings.

A block diagram of a transcutaneous energy transfer system is shown in Figure 1.1. A transcutaneous energy transfer system consists of a transcutaneous transformer, a coil-driver, a rectifier, a transcutaneous data transmission system and some control circuitry. The basic operation of a transcutaneous energy transfer system is as follows. The coil-diver produces an alternating current through the primary coil. This alternating current, in turn, produces an alternating magnetic flux in the primary coil. The portion of the alternating magnetic flux, captured by the secondary coil, induces an alternating voltage across this coil according to Faraday's law. An alternating current will flow through the secondary coil as the result of this induced voltage. Since most of the implanted medical devices need to be supplied by direct current (DC), this alternating current is required to be changed to direct current by the rectifier block. To regulate the output voltage, a voltage control loop is employed. The transcutaneous data transceiver delivers the information of output voltage level

to the exterior of body where it is used to determine the amount of current required to be driven to the primary coil for keeping the output voltage fixed [3, 1].

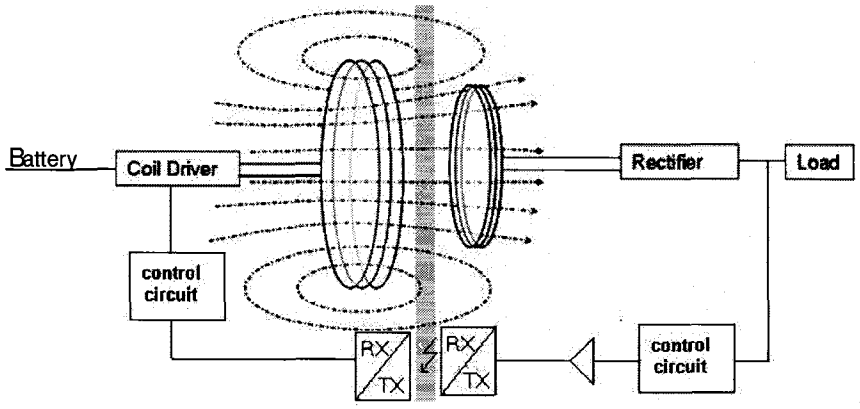

Figure 1.1 A transcutaneous energy transfer system block diagram [3]

Although the early efforts to design a transcutaneous energy transfer system is referenced back to 1960 [6], the main contributions to this technology, as the paper review suggests, have been made after 1980 [1]-[7]. Among the contributions made to enhance the design of a transcutaneous transformer, Soma [8] introduced an algorithmic analytical method for designing a transcutaneous transformer. He also introduced the Geometrical method for partially desensitizing a transcutaneous transformer to lateral displacements of its coils. Zienhofer and Hochmair [9] introduced the Enhanced Geometrical method, a technique which increases the overall efficiency of a transcutaneous transformer. Critical coupling is a method invented by Hochmair [10]. By applying this method maximum voltage could be induced in the secondary side of a transcutaneous transformer while a convenient coils separation distance between the two coils can be maintained. Galbrith et. al. [11] introduced the "Stagger tuning" method. With this method the desensitizing of voltage gain of

two coupled coils to the variation of the coupling coefficient of the two coils is possible. Eierhofer et. al. [12, 13] proposed a Class-E coil-driver circuit that can track the varying separation-distance of the two coils of a transcutaneous transformer for maximum power transfer efficiency.

To induce a voltage in the secondary coil of a transcutaneous transformer, a proportionate current must be driven to the primary coil. Several techniques have been developed for driving the current to the primary coil of a transcutaneous transformer most efficiently. The series resonant coil-driver is one of those methods. Ghahari [2], Kim [14] and Joung [4] used the series resonant coil-driver for designing a transcutaneous energy transfer system. Instead of using a pancake shape coils for a transcutaneous transformer, they used coils wound on ferrite pot-core, just for experimental purposes. Ghahari applied the theory of series resonance to the primary side of the transcutaneous transformer to improve the voltage gain of a transcutaneous transformer, however the voltage gain and efficiency he obtained were 0.165 and 50% respectively. Kim employed resonance on both the primary and the secondary sides of the transcutaneous transformer. He used the pulse-width modulation method to control the output voltage. The voltage gain he obtained was improved to 1.1. Joung also employed resonance at both the primary and the secondary coils but used the frequency variation method to control the output voltage. The voltage gain and efficiency he obtained were 0.4 and 70% respectively. Nishimura [15] used pancake-shape coils for transcutaneous transformer for a series resonant transcutaneous energy transfer system, however the best efficiency he obtained was 45%.

An alternate technique to design a coil-driver is using the Class-E amplifier that is

invented by Sokal [16]. Troyk [17] analyzed the application of a Class-E amplifier as a Coil-driver for a transcutaneous energy transfer system. Wang et. al. [1, 18] designed a transcutaneous energy transfer system with a Class-E coil-driver whose output voltage is controlled by variation of input voltage. This system has an efficiency of 65% for the coil separation-distance of 7 mm. Puers [3] also used the same method to design an output voltage regulated transcutaneous energy transfer system. Miller et. al. [5] introduced a frequency-tracking with Class-E coil driver system. This system has an efficiency of 83% for the coil separation-distance of 5 mm.

Designing a reliable and efficient transcutaneous energy transfer system is the main subject of this thesis. This thesis presents a study on feasibility and design of a transcutaneous energy transfer system based on a Class-E power amplifier coil-driver in which frequency variation is used as the main tool to control the output voltage.

1.1 Motivation

The main motivation behind the subject of this thesis is to try to make a contribution to the technology of transcutaneous energy transfer systems toward the goal of improving quality of life for the instances that deteriorating health condition has provided hard condition for human being.

The frequency-controlled Class-E transcutaneous energy transfer system, among other methods, has specific features that have made it a promising method to design a transcutaneous energy transfer system.

1.2 Objective

The objective of this thesis is to investigate and design a frequency-controlled Class-E transcutaneous energy transfer system. To achieve this objective the following steps are carried out.

- A circuit for the frequency-controlled Class-E transcutaneous energy transfer system is introduced
- The proposed circuit is analyzed
- The system is mathematically modeled using MATLAB
- The system is simulated using PSPICE
- A prototype is constructed and tested
- The simulation results are verified by the experimental results
- The challenges for designing a system with this method are identified
- The advantages and disadvantages of this approach over the previous work in terms of design reliability and efficiency are identified

1.3 Thesis Organization

This thesis contains a survey of the relevant literature and challenges on transcutaneous energy transfer system design in Chapter 2. Chapter 3 introduces the concept of the transcutaneous transformer and its electrical equivalent circuit. In Chapter 4, the Class-E amplifier as well as the Class-E rectifier are introduced and expressions that govern their operation are outlined. These expressions are used for modeling the coil-driver as well as the rectifier building blocks of the system. In fact Chapters 3 and 4 provide the necessary information needed for analysis of the proposed system. In Chapter 5, our proposed transcutaneous energy transfer system is introduced, its

circuit analysis is performed and the transfer function of the final system is derived and interpreted. Chapter 6 uses the results of Chapter 5 to conduct the simulations needed to find the regions of the transfer function which are safe for system operation. This chapter concludes with the results of experiments conducted on a prototype system and the explanations for the discrepancies with the simulations results. Chapter 7 presents a summary of the thesis, some concluding remarks, contributions made, and some guideline for future work.

Chapter 2

TRANSCUTANEOUS ENERGY TRANSFER SYSTEM DESIGN: A REVIEW STUDY

In this chapter the transcutaneous energy transfer system is studied through a literature review. At first the technologies for each of the most important blocks of a typical transcutaneous energy transfer system such as the transcutaneous transformer, the coil driver and the rectifier are reviewed and finally the various transcutaneous energy transfer systems will be briefly introduced .

2.1 Transcutaneous Transformer

A transcutaneous transformer is composed of two pancake shape coils which are placed opposite to each other. Figure 2.1 shows the two coils of a transcutaneous transformer.

This transformer has a very poor coupling since there always exists a gap of around 0.5 to 2 cm between its two coils depending of the thickness of the skin tissues. This gap limits the amount of flux captured by the secondary coil and reduces the coupling coefficient of the transformer. The uncoupled portion of the flux can be represented

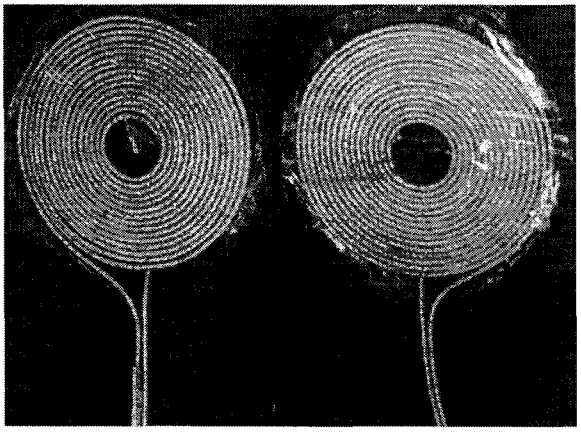

Figure 2.1 Coils of the transcutaneous transformer used in this thesis

by a separate self inductance that is called the leakage inductance [2].

2.1.1 Transcutaneous Transformer Equivalent Circuit

Figure 2.2 represents the two coils of the transcutaneous transformer. In this figure L1 and L2 are the self inductances of the primary and the secondary coils and the resistors R1 and R2 are the equivalent series resistance of the primary and the secondary coils respectively.

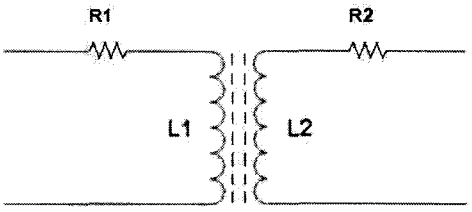

Figure 2.2 A model for transcutaneous transformer

The T equivalent circuit of the transcutaneous transformer, when the resistive losses of the coils are neglected, is shown Figure 2.3. LL1 and LL2 are the leakage inductances of the primary and the secondary sides respectively and LM represents

the coupling inductance of the transcutaneous transformer. In fact to account for the stranded flux which doesn't close its path through the secondary coil, more than the required flux to pass through the secondary coil is needed is to be produced by the primary coil. The existence of this extra flux which requires extra current at the primary side, which is called magnetizing current, is represented by the coupling inductance LM in the equivalent circuit. The relationship among the self-inductances of the two coils, L1 and L2, the leakage inductances LL1 and LL2, the coupling inductance LM and the coupling coefficient of the transcutaneous transformer, k, are [2, 10]:

$$LM = k\sqrt{L1 \cdot L2} \tag{2.1}$$

$$LL1 = L1 - \frac{LM}{n} \tag{2.2}$$

$$LL2 = L2 - LM \cdot n \tag{2.3}$$

The leakage inductances prevent the circuit from having a large voltage gain since part of input voltage drops on them. Large magnetizing current prevents the transformer from having a good efficiency. Specific coil driving techniques are required to minimize the effects of the large leakage inductances.

2.2 Transcutaneous Transformer Design

This section presents the major techniques for designing a transcutaneous transformer. Some of these techniques are general and some are particular methods to alter a particular characteristic of a transcutaneous transformer.

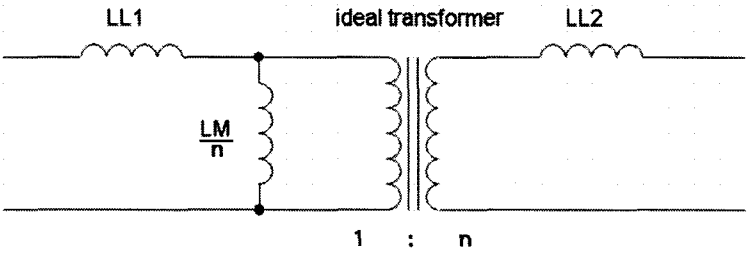

Figure 2.3 A model for transcutaneous transformer

2.2.1 Transcutaneous Transformer Design and Coil Based Regulation

Soma [8] introduced a simple and efficient mathematical approach to design a transcutaneous transformer which is generally described here without going into mathematical details. As the first step the coupling coefficient of two circular, single-turn coils, in their different mutual positions are determined. The different mutual positions of the two single-turn coils are illustrated in Figure 2.4. This task requires one to determine the mutual inductance between these two coils. The equation of mutual inductance between two single-turn coils is a classic electromagnetic equation that is available in relevant text books. Soma developed an approximate equation, instead of the exact equation, for the mutual inductance between the two single-turn coils and extended the solution to cover the lateral, angular and eventually both of these misalignment cases. This solution is claimed to be accurate within 10% of the value obtained by the exact equation.

To extend the equation for a real coil which is composed of multiple single-turn coils, the real coil is modeled as a single turn coil times an "average dimension". For example, for a pancake-shape coil, the average dimension would be the arithmetic mean of the radii of all the single-turn circular coils available in the coil. After the

approximate coupling coefficient of a real coil is determined, the following algorithm is used to design a real coil:

- Determine coils parameters based on system consideration such as implant location etc.
- Determine nominal and worst-case angular and lateral displacement
- Assume a structure for the coil in the allowable parameters range
- Determine coupling coefficient with the method just described
- If coupling coefficient does not meet other design goals (bandwidth, gain ,..) change the parameters and iterate until the desired coupling for the coil is reached

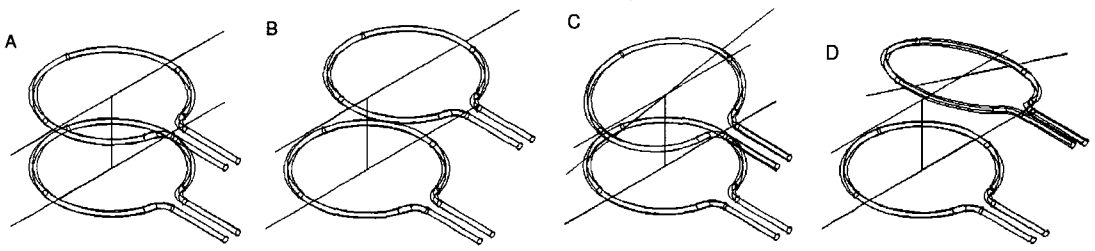

Figure 2.4 Different mutual positions of two one turn coils A) Two concentric coils with only separation distance B) Two coils with lateral misalignment C) Two coils with angular misalignment D) Two coils with lateral and angular misalignment

2.2.2 Geometrical Approach

The geometrical approach is used to desensitize an inductive link gain to coil lateral misalignments. In this approach, as illustrated in Figure 2.5, the external coil is larger than the implanted coil and as long as the smaller coil remains within the perimeter of the larger coil, the flux line that is shared by both of the coils will be roughly the same, and the coupling will remain fairly constant. Thus, the coils can

move laterally and even tilt with only a minor effect on the gain. A transcutaneous transformer designed by this approach is still sensitive to changes in distance between the coils. In exchange for partially controlling the gain, the magnitude of the coupling is sacrificed, since these coils share fewer flux lines than equally sized coils. A lower coupling coefficient requires higher current in the primary coil to provide the same output power at the secondary coil. The higher current at the primary coil also causes more resistive loss in this coil. A poor bandwidth is another problem, since to maintain a high gain, the link must have a high quality factor, Q, which results in a smaller bandwidth [8].

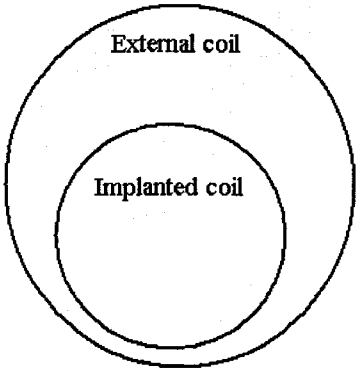

Figure 2.5 Coils relative sizes in geometrical approach

2.2.3 Enhanced Geometrical Approach

The coupling between the two magnetically coupled coils can be enhanced by distributing the turns of the coils across the radii instead of concentrating them at the outer circumference. This method of winding a coil is called "advanced geometrical approach". In exchange for the coupling enhancement, there would be a moderate decrease of the unloaded quality factors of the coils due to the increased wire length.

But if unloaded quality factors are sufficiently high compared to the loaded quality factors, the effect of the coupling enhancement predominates the effect of the unloaded quality factor reduction on the overall efficiency and thus a net improvement of the overall efficiency is obtained [9].

2.2.4 Critical Coupling

Hochmair [10] defined a special method of coupling two coils which is called "critical coupling". By critically coupling it would be possible to reduce the effect of coils separation and lateral displacements. Critical coupling also makes it possible to obtain maximum induced voltage with a convenient coil separation distance despite steep decrease of the magnetic field with increase of the separation distance between the coils. In exchange for this advantage, there would be a theoretical 50% reduction in the energy transfer efficiency.

The critical coupling coefficient, K, as opposed to conventional coupling coefficient, k, defined in 2.4.

$$K = k\sqrt{Q_1 Q_2} \tag{2.4}$$

In this equation Q_1 and Q_2 are the primary and the secondary quality factors and k is the conventional coupling coefficient of the two coils. It is said that the two coils are critically coupled when critical coupling coefficient,K, is unity.

2.2.5 Stagger Tuning

The stagger tuning approach is used to desensitize the voltage gain of two coupled coils to the coupling coefficient of the coils. In this technique, in the transfer

function of the link, one pole is placed above the operating frequency and one pole below it. The poles move as the coupling coefficient changes. If the poles are placed properly, their positions move in a way to compensate the gain drop due to the coils' coupling changes. In this way the coils could be misaligned in a realistic manner with little effect on the output transferred power. This approach provides both efficiency and bandwidth, the two characteristics which were mutually exclusive in the earlier mentioned approaches. Besides, in this approach the coils are equally sized, which improves the average coupling and reduces the coils' resistive losses. Another point is that the stagger tuning can not be employed in a Class-E coil-driver, since a Class-E loses efficiency if the load does not resonate at the operating frequency, instead a Class-D amplifier can drive this load because it is independent of the frequency [11].

2.3 Coil-Driver Technologies

A coil-driver circuit is needed to supply enough current to the primary coil to enrich the share of flux which pass through the secondary coil to the required value providing a certain amount of voltage and power at the output. The voltage gain of the system is very sensitive to the leakage inductances of the primary and the secondary coils due to the drop of a part of the input voltage on these leakage inductances. By using proper coil-driver techniques these unwanted voltage drops across the leakage inductances could be eliminated and accordingly the voltage gain of the system could be increased. These techniques, among them the "series resonant" and the "Class-E" coil-drivers, incorporate the leakage inductance of the transcutaneous transformer into one resonant circuit to reduce its effect at the resonance frequency.

2.3.1 Series Resonant Coil-Driver

By incorporating a leakage inductance into a series resonant network, the effect of leakage inductance on the voltage gain of the system at the resonant frequency is eliminated. Figure 2.6 shows a circuit in which the resistor R, which is the output load, is supplied by an AC voltage source through a series resonant network. In fact the capacitor C is placed in series with the inductor L to cancel its effect at the resonant frequency. At this frequency the voltage gain, which is the ratio of the load voltage to the input AC voltage, is maximum and the input impedance seen from the AC source is minimum.

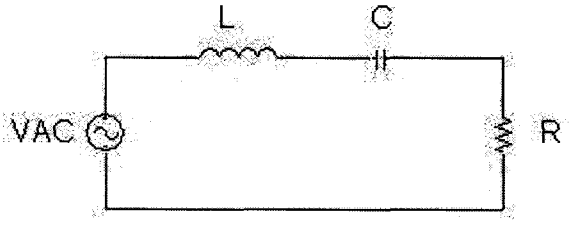

Figure 2.6 A series resonant network

By replacing the input AC voltage of the circuit of Figure 2.6 with a switching network and also the resistive load of that circuit with a series combination of a rectifier and a filter capacitor, the circuit of Figure 2.7 is realized. This circuit is a series resonant converter [19]. The switching network of this circuit works as follows. The transistors M1 and M4 are on for 50% of a period while the transistor M2 and M3 are off, applying the input DC voltage on the resonant network. On the next half period, the transistors M2 and M3 are on while the transistors M1 and M4 are off, applying the inverse of input voltage on the resonant network. In this way an AC

square wave voltage is applied to the series resonant network where its main harmonic is rectified, filtered and the resultant dc voltage is delivered to the load.

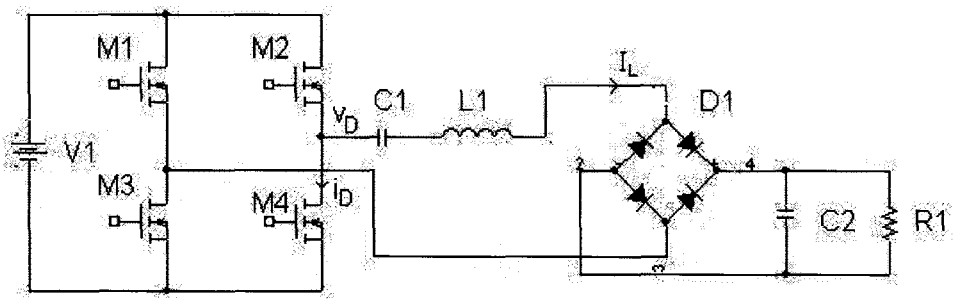

Figure 2.7 A series resonant converter

One of the main sources of power transfer deficiency and internal power losses in this converter is the switching losses of the transistors. During the time that a switching transistor is on or off, either of the transistor voltage or the current flowing through it is zero, making the power loss of the transistor zero. But at the switching time, for example at the turn-on state, the current of the transistor linearly raises from zero to a maximum and the voltage across it changes from a maximum to zero, therefore, the power loss which is the product of these current and voltage is not zero. By applying special techniques in series resonant converters, either of the turn-on or turn-off switching losses is eliminated and accordingly the efficiency is increased. Figure 2.8 shows the drain voltage and current of transistor M4 as well as the load current, I_L, of the circuit in Figure 2.7 when the circuit is operating at exact resonant frequency of the series resonant network of L1 and C1.

As seen, the transistor current at switching instances is zero which will result in zero switching losses of the transistor, however, when there is a slight frequency

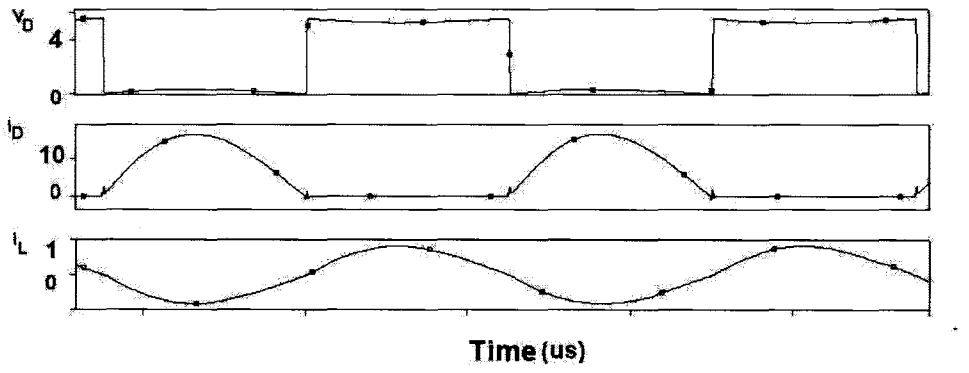

Figure 2.8 The drain voltage and current of transistor M4 and the load voltage of the series resonant converter of Figure 2.7 when it is operating at its exact resonant frequency

deviation, this condition will not be maintained. If operating frequency is higher than the resonant frequency of the series resonant network, the series resonant network acts like an inductor and consequently the current flowing through resonant inductor lags the voltage applied to the resonant network and therefore the waveforms of the Figure 2.9 result.

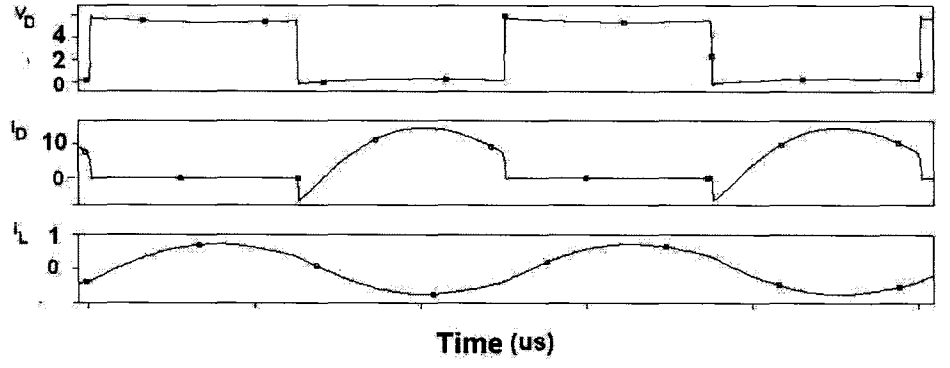

Figure 2.9 The drain voltage and current of transistor M4 and the load voltage of the series resonant converter if Figure 2.7 when its operating frequency is less than its resonant frequency

From this figure it is seen that no turn-on switching losses exist in the transistor since the voltage across the transistor is zero before it conducts current. The nega-

tive i_D current seen in this figure is caused by turning off of the opposite transistor M2. That is when the transistor M2 turns off, the current of the resonant inductor flowing through this transistor is transiently maintained by the inductive action of the resonant inductor. This current is then forced to come up through the transistor M4 in reverse direction or through its antiparallel parasitic diode [20].

Although this method eliminates the turn-on switching losses, the turn-off switching losses is only reduced by placing a lossless capacitor, called snubber capacitor, across each of the transistors. Actually, in this circuit, no snubber discharge resistor is needed since these capacitors are discharged by the inverse current due to the inverse action of the inductors when the corresponding opposite transistor in the bridge turns off. This state happens as opposed to the case where these capacitors are discharged through the snubber resistor when the corresponding transistor turns on. For example when the transistor M2 turns off, the resonant inductor current which is forced to flow through the transistor M4 in reverse direction, will also discharge the snubber capacitor across the M4 transistor.

Considerable switching losses are also attributed to the charging of the switching transistors' drain-source and drain-gate parasitic capacitors and discharging them with the turn-on action of those transistors. In series resonant converters operating above the resonant frequency of their resonant network, however, these parasitic capacitors are not discharged by the transistors themselves, but by the transient reverse current caused by turn-off of their corresponding opposite transistors in the bridge network. This happens by the same argument as stated before, that is, the parasitic capacitors charges are returned to dc source by virtue of the reverse current

conduction of their corresponding opposite transistors due to the inductive action of the resonant inductor.

The other option would be to choose the switching frequency lower than the resonant frequency of the series resonant network. In this case the turn-off switching losses of the transistors are eliminated, however, reducing the turn-on losses is not as easy as placing a snubber capacitor across each switching transistor but require placing small inductors in series with each transistor. The switching losses associated with the parasitic capacitor's energy storage are high since these devices' capacitors are discharged by their corresponding transistors turn-on action instead of by the opposite transistors inverse current [20].

The theory of series resonant inverter could be employed to design a series resonant transcutaneous energy transfer system. Figure 2.10 shows a series resonant transcutaneous energy transfer system.

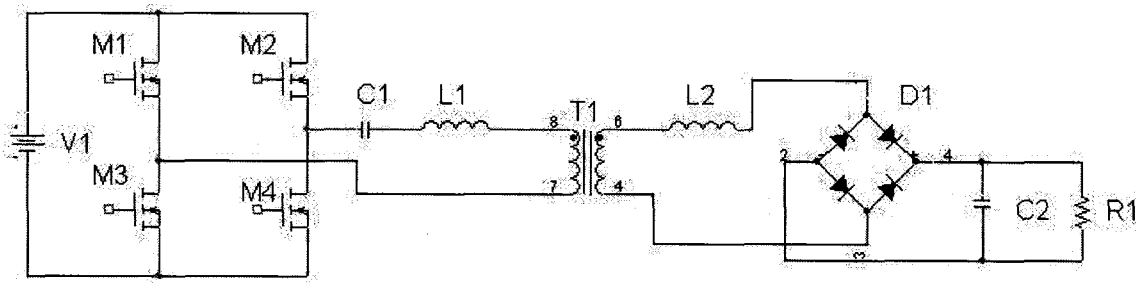

Figure 2.10 A series resonant network [19]

In this figure the leakage inductor of the transcutaneous transformer has taken the place of the resonant inductor at the primary side. By employing the series resonance theory at the secondary side, the leakage inductance at this side could also be eliminated. In Section 2.4 a literature review of the related work is performed. This

review presents the results of applying the series resonance theory on the secondary side [2], the primary side [15] and both sides of a transcutaneous transformer [4, 14].

The series resonant transcutaneous energy transfer system has high voltage gain and therefore doesn't require a high voltage battery at the primary side. However, applying a small voltage to the input requires the driver to handle a large amount of current to supply the load with the required amount of power at the output. Since the equivalent series resistance of a series resonant transcutaneous energy transfer system is extremely low at resonant frequency, the conduction loss of its switching transistors would be dominant and excessive. To reduce the conduction loss of the switching transistor, it is necessary to use a transistor with extremely low on-state resistance for the driver. However, low-resistance devices tend to have large die area and would be characterized by large input capacitance and this raises the power handling requirement of pre-driver stage. Another option would be to employ a parallel resonant transcutaneous energy transfer system [17]. The fact is that a parallel resonant network has a large equivalent resistance at the resonant frequency, thus although the resistive losses across the transistors are not dominant, but a large input voltage is required to supply the necessary current to the input for the required output power, and in addition to that, a high voltage transistor also has the same power handling problem as mentioned for high current transistor. A combination of parallel and series resonant networks might produce a perfect solution for this problem. This leads to the fundamentals of the theory of Class-E coil-driver which is discussed on the following sub-section.

2.3.2 Class-E Coil-Driver

A Class-E coil driver is basically a Class-E power amplifier used for driving current through a coil. A Class-E amplifier circuit is principally a multi-frequency resonant network whose circuit is shown in Figure 2.11. The multi-frequency circuit has two resonant frequencies. These resonant frequencies are the series resonant frequency of the series L2 and C2 elements and the parallel resonant frequency of the equivalent inductance of the series L2-C2 and the C1 capacitor. The input impedance versus frequency of this circuit is shown in Figure 2.12.

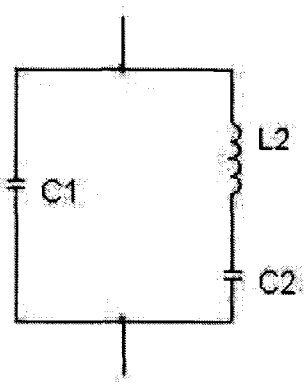

Figure 2.11 The multi-frequency network

The valley in impedance in this figure is caused by the resonance of L2 and C2. At higher frequencies, positive inductance of combination of L2 and C2 forms a parallel resonant network with C1. At a particular frequency between the series and the parallel peaks the multi-frequency network exhibit a favorable load condition for a switching transistor driving this circuit. At this frequency the power losses in this transistor are minimized and it operates at both moderate current and voltage. This point is called the Class-E operating point [17].

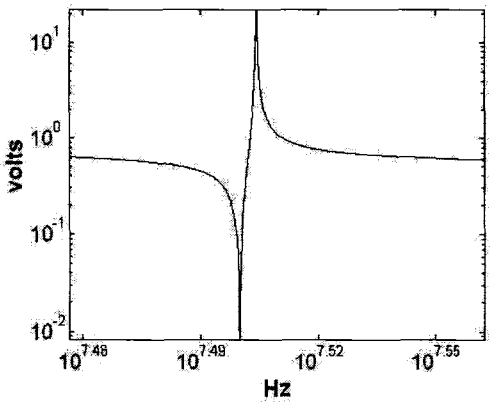

Figure 2.12 The frequency response of the multi-frequency network

Figure 2.13 shows the circuit of a Class-E coil driver. In this figure, the C2-L2 branch is a high quality "Q" series resonant network thus the current flowing through it is nearly sinusoidal with a frequency equal to the switching frequency.

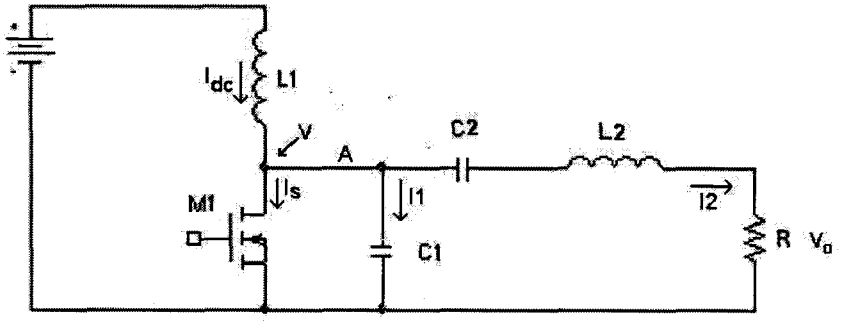

Figure 2.13 A Class-E coil-driver

While the switch is closed, L2 and C2 supply the current back to the switch. When the switch is open, L2-C2 continue supplying current, however this time through C1, resulting in a positive voltage across the switch. When this current reverses, the charge on C1 supplies the current, reducing the voltage across the switch. When the voltage across the switch becomes zero, the switch is closed and the cycle is repeated.

In this figure L1 acts as a current source, supplying the energy being dissipated during each cycle.

At the Class-E operating point, the switch voltage and L2 current are 90 degree out of phase and the voltage across the switch is zero with zero slope at transistor closure time. This ensures there will be no large peak current at the switch in the switching instances therefore the switching losses across the driver transistor are minimized. The Class-E operation point is only maintained at a particular Q of the multi-frequency network in which the output load resistance, R, is also included. Figure 2.14 shows that for low values of this Q, ringing of the voltage across the transistor, when it is turned off, is excessively damped, resulting in a negative peak above zero. For high values of this Q, the ringing of the switch voltage does not sufficiently damp and would cause the switch voltage to have a negative peak below zero. At a particular Q, which is called the critical Q, the ringing of the switch voltage returns to zero at zero slope. When the circuit is operating at the Class-E operating point, it is possible for the switch transistor to switch at the instances when not only the voltage across the switch but also the slope of this are zero.

The zero-voltage switching of driver transistor prevents a large current surge in the switch and the zero-slope switching allows for slight timing error or slow switch closure. In fact zero-voltage and zero-slop switching of the driver transistor are the main features of a Class-E amplifier and should be kept during all working condition of an amplifier. However, there are some factors that may throw the circuit out of the Class-E operating point such as inductance and load variations. Troyk [17] has introduced a Class-E amplifier circuit that controls either frequency or duty cycle of

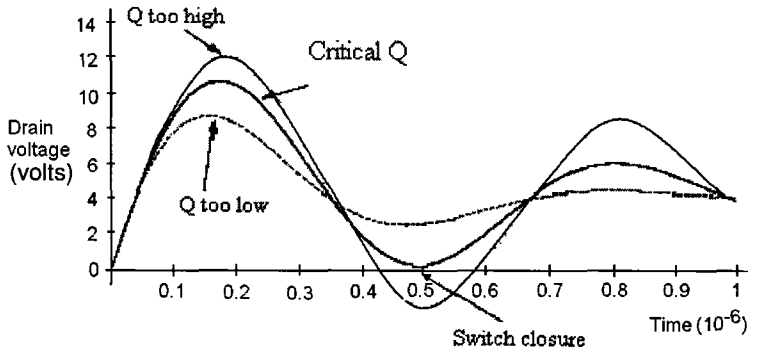

Figure 2.14 The voltage oscillations across the transistor in a Class-E amplifier when it is turned off for different load network quality factors

the driver transistor to accommodate the circuit for the Class-E operating point when the load or the series inductance of the Class-E amplifier are varied. This circuit is using this fact that the current in the series inductor is the derivative of the switch voltage (when the LC branch is starting to get capacitive), therefore by detecting the zero current crossing of the the series inductor, which is sensed by a small pulse transformer, switch closure instant is determined. By keeping the switch on-time fixed, the controlling of the switch closure would control the operation frequency of the circuit and thereby the Class-E operation mode is maintained.

One other feature of a Class-E amplifier is that its operating frequency is not limited by the parasitic capacitors of the driver transistor. The drain parasitic capacitor in a power amplifier is usually a limiting factor for increasing the switching frequency since it takes time to be charged and discharged. In Class-E amplifiers this capacitor can be incorporated into the capacitor C1 in the design phase thereby its impact on increasing the operation frequency is removed [17, 16].

As an application of Class-E amplifier in a coil-driver, Eierhofer et. al. [12, 13]

introduced a Class-E coil-driver circuit which can track the separation-distance of the two coils of a transcutaneous transformer for maximum power transfer efficiency. This circuit is shown in Figure 2.15. While the two coils of the transcutaneous transformer, L2 and L4, are coupled with coupling coefficient of k, they have a coupling with transistor driving coil, L3, for self oscillation purpose. This coupling is represented by coupling k1 between L2 and L3 coils in this figure. The oscillation frequency of this circuit is influenced by the mutual position of the coils. The coupling variations of these coils produce a frequency offset which tracks the spectral location corresponding to the absolute maximum power transfer efficiency. In this way an automatically tuned power amplifier for maximum power transfer with varying separation-distance between the two coils of a transcutaneous amplifier is realized.

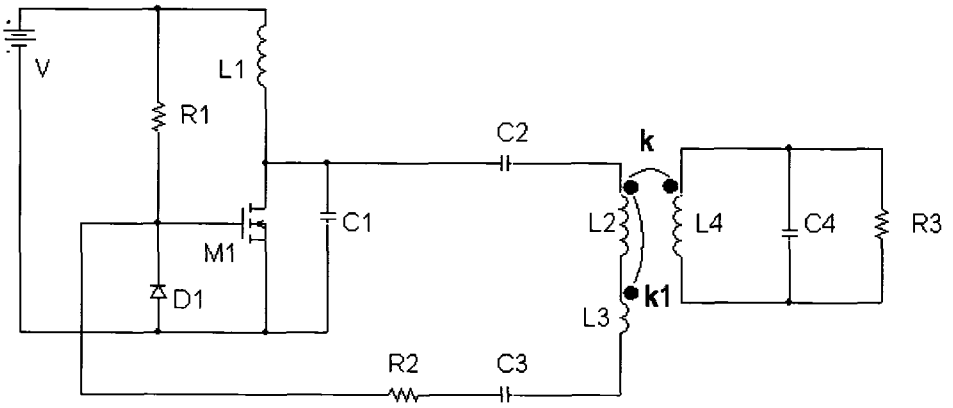

Figure 2.15 A self-tuning Class-E coil-diver

2.4 Previous Work for Designing a Transcutaneous Energy Transfer System

The previous work concerning designing a transcutaneous energy transfer system so far presented in the literature could be classified based on either the type of the coil-driver employed or the particular transcutaneous transformer used or even the rectifier and output filter utilized. Here a classification based on the type of coil-driver is used since changing the type of coil-driver of a transcutaneous energy transfer system has more over-all impact on the design method and the performance of the designed transcutaneous energy transfer system than any other part of a transcutaneous energy transfer system. In this way the main classes identified are a transcutaneous energy transfer system with a series resonant coil-driver, a transcutaneous energy transfer system with a Class-E coil-driver and finally a transcutaneous energy transfer system called frequency-tracking or auto-tuned transcutaneous energy transfer system.

2.4.1 Series Resonant Coil-Driver Transcutaneous Energy Transfer Systems

Several methods have been introduced to design a transcutaneous energy transfer system based on series resonant network. Ghahari [2] introduced a transcutaneous energy transfer system in which series resonant technique is applied on the secondary side of the transcutaneous transformer. He argues that since in a transcutaneous transformer the coupling inductance is not large compared to the secondary leakage inductance, a significant portion of the primary current flows back to the source through this inductance and is wasted. Reducing the secondary leakage inductance reduces the impedance seen in parallel with the coupling inductance and hence helps

the input current to flow to the secondary side and load rather than short circuiting at the primary side. The voltage gain that Ghahari obtained was 0.165 and his efficiency was 50%. Following this work, Kim [14] employed resonance on both the primary and the secondary sides of the transcutaneous transformer. He practically found out that if the secondary resonant frequency is smaller than the operating frequency, the current flow to the coupling inductor of the transcutaneous transformer is minimized. In Kim's work the variation of the duty-cycle of the pulses driving the switching transistor was used to control the output voltage and in his circuit the components' values were determined through an intuitive simulation approach. The voltage gain he obtained was improved to 1.1 while there is no indication of efficiency value obtained in his work . Joung [4] did the most comprehensive work on the series resonant approach by employing resonance at both the primary and the secondary sides and using the frequency variation to control the output voltage against the coupling and the load variations. The best voltage gain he achieved is 0.4 and his system's best efficiency was 70%. In all these aforementioned cases a ferrite pot core was used as transcutaneous transformer which is not suitable for implantation as a pancake shape coils is. Nishimura [15] designed a series resonant transcutaneous energy transfer system with pancake-shape coils whose coupling was enhanced by using an amorphous core which is a flexible material with properties close to ferrite core. However the best efficiency he archived was 45%.

2.4.2 Class-E Coil-Driver Transcutaneous Energy Transfer Systems

Wang et. al. [1, 18] designed a transcutaneous energy transfer system with a Class-E coil-driver. In this system the varying input voltage is used to account for coupling and load variations. A DC-DC converter provides the varying input voltage for this system. The designed system transfers 250 mW of power to a cochlear implant. The best power transfer efficiency achieved by this transcutaneous energy transfer system is 65% for a coil distance of 7mm. The same approach is also used by Puers [3] for output voltage regulation of a transcutaneous energy transfer system. Although this method simplifies the design of a transcutaneous energy transfer system, it increases the weight of the total system due to the need to have a DC-DC converter in the front side and likewise degrades the overall efficiency due to the losses in the DC-DC converter.

2.4.3 Frequency-Tracking Transcutaneous Energy Transfer System

Miller et. al. [5] introduced a transcutaneous energy transfer system with a particular circuit structure which is called "Frequency-Tracking" or "Auto-tuned" transcutaneous energy transfer system . Figure 2.16 represents the schematic circuit of the main power transfer part of this system.

In this figure L2 and L4 represent the leakage inductances of the primary and secondary side of the transcutaneous transformer. R1 represents the load and L1 and L3 represent the mutual inductances between the primary and secondary coils which have a coupling coefficient of K. The capacitor C1 tunes the primary coil to a specific frequency whose value depends on the primary leakage inductance. The transistor

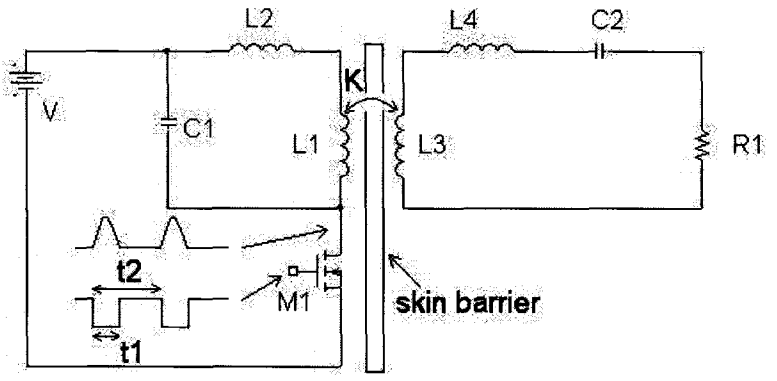

Figure 2.16 The frequency-tracking transcutaneous energy transfer system

M1 is driven with a rectangular waveform with period t2 and off-time duty cycle of t1. The primary coil oscillates at its resonant frequency (f_p) which depends on the coupling conditions of the transcutaneous transformer when the transistor M1 is off. To prevent clipping of the primary voltage waveform, the primary resonant period ($1/f_p$) is constrained to be larger than t1 at its lowest value i.e. under maximum coupling and smaller than twice t1 at its highest value i.e. under minimum coupling. The secondary coil is tuned by capacitor C2 to the frequency of $f_s = 1/t2$ or the primary switching frequency. This state is called "in-tune" as opposed to the "off-tune" state in which the resonant frequency of secondary side circuit is not equal to switching frequency.

As the coils separation-distance varies, the secondary leakage inductance is varied and accordingly the resonant frequency of the secondary coil changes. If the primary circuit keeps driving at the fixed frequency of $f_s = 1/t2$, then the secondary circuit gets off-tune, leading to the introduction of an inductor to the secondary circuit and a voltage drop across it accordingly. As a result the voltage seen by the load is reduced. This makes the power delivered to the load extremely sensitive to the coils

separation-distance. To compensate for it the switching frequency of the primary side circuit must be changed.

To sense the coils separation-distance variation, it is argued that the primary current is composed of two component, one is attributed to the primary current of the primary coil and the other is attributed to the reflected coil current from the secondary coil. Since the change of resonant condition at the secondary side introduces the proportional inductance at this side, this condition, when transferred to the primary side, could be detected by phase difference changes between the primary current and voltage at this side. The change of phase could be used to change the frequency of the rectangular waveform driving the transistor at the primary side to keep the secondary side always "in-tune"

Chapter 3

TRANSCUTANEOUS TRANSFORMER

A transcutaneous transformer is the component with which the power for an implanted device is transferred through the skin. It is composed of two coils. Since one of these coils is implanted under the skin, there is a separation distance as large as the skin thickness between them. This separation distance significantly reduces the coupling between the two coils and accordingly increases the leakage inductances at the primary and secondary sides. A good transcutaneous transformer, other than being implantable, should have the best coupling coefficient for a specified separation distance and accordingly the smallest leakage inductances. Although the leakage inductance will never be reduced to zero, however, their effect is totally eliminated by employing some circuit techniques which will be discussed in Chapter 5.

In this chapter, first a method is introduced to identify the main characteristics of an assumed transcutaneous transformer, such as the number of turns and the pitch size, by simulation. After the coils are wound, a measuring method is introduced to calculate the characteristics of the wound transcutaneous transformer which will

lead to a determination of the elements of the electrical model of the transcutaneous transformer. This also will be useful for verification of the simulation results.

3.1 Introduction

The flat pancake shape structure is the most popular transcutaneous transformer used for a transcutaneous energy transfer system [24, 25, 26]. Its flatness makes it convenient to be implanted under the skin with minimum separation distance between the two coils and the roundness makes it easy to wind and prevents flux leakage at the edges as opposed to other alternative shapes. Several studies have been conducted to determine the number of turns, radii of minimum and maximum loops in a coil and the structure of the wire with which to wind the coils [8, 9, 11, 21].

Increasing the coupling coefficient of two coils in a transcutaneous transformer is the main concern of any design since it helps to reduce the primary current for the same output power which accordingly reduces the primary power loss of I^2R and increase the overall efficiency of a transcutaneous energy transfer system. Increasing the outer diameter of both primary and secondary coils equivalently helps to increase the coupling between the two coils [21] however the size constraint imposed by the maximum allowable implantation area available for each application determines the diameter of the secondary coil. Once the size of the secondary coil is determined the size of the primary coil, required winding wire and winding method can be found accordingly. On the other hand to reduce the coils resistances it is best to use a special kind of wire known as Litz wire. A Litz wire is made from hundreds of strands of very thin insulated wires. At operation frequency of a transcutaneous energy transfer

system which would be some hundreds of kilo hertz, according to skin effect, current tends to flow through the thin outer layer of any wire and thus the core of the wire would be left useless and conduct no current. Using multiple thinner wire instead of a thick wire actually helps to effectively use the whole cross sectional area of a wire for current conduction and reduces wire resistance at high frequency.

Through an analytical approach Zienhofer and Hochmair [9] have shown that when the radius of the minimum loop in a coil is less than 40% of the maximum loop there would be no increase in the coupling coefficient of the two coils. This finding is subsequently verified by Atluri [21] by a simulation approach. This fact suggests that if the turns of the wire loops in a coil are smoothly distributed across the coil radius with a fixed winding pitch, the resulting coils have better coupling coefficient when compared to the case where the turns are concentrated at the circumferences. The same work [21] also suggests that the winding pitch size doesn't have any significant effect on the resulting coupling coefficient (but effective on the inductance of the coil).

Once the geometry of the coils are determined, to design the coils for a particular coupling and inductances, one can resort to simulations techniques that will be illustrated in the following section and once the coils are wound, through particular measurement and analysis method which is elaborated in Section 3.3 the characteristics of the coils can be verified.

3.2 Transcutaneous Transformer Design Through Simulation

When the distance between two coils as well as their diameter are assumed to be fixed, the number of winding loop-turns and winding pitch for optimum self and cross

inductances can be found by simulation. There are several tools for coil simulations but what is used here is the full wave electromagnetic simulator HFSS from Ansoft company. The software is quite strong for defining the geometry of the coils as well as analyzing and computing the self and mutual inductances of the coils and their coupling coefficient. Through the simulations not only can the techniques suggested in the previous section be investigated, but also for a coil with particular diameter, different winding pitch or turning loops can be tested to find the best self and mutual inductances for a particular design.

3.2.1 Drawing a Spiral Coil in HFSS

HFSS has a special tool for drawing any desired spiral coil with a circular cross-section wire. Figure 3.1 shows a spiral coil which is drawn in this way. There is one

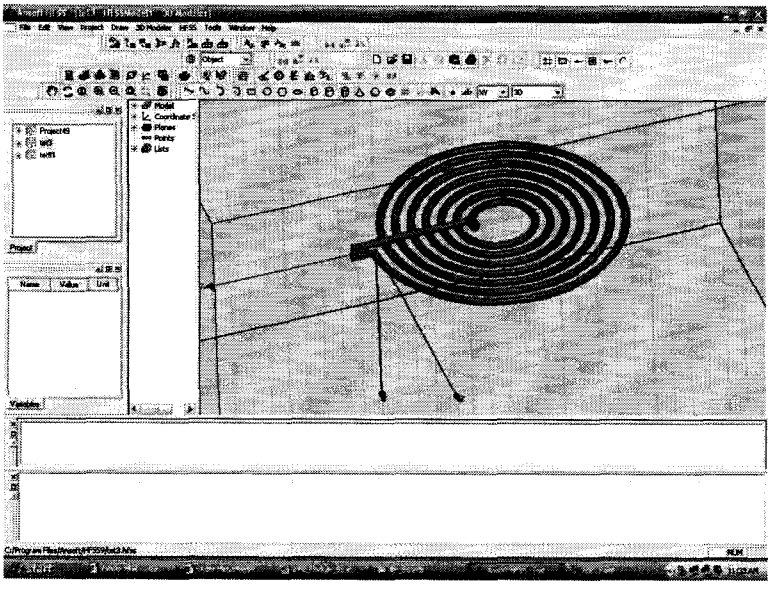

Figure 3.1 Simulation of spiral coil in HFSS environment

problem with the spiral coil produced in this way which requires very long analysis

time and often the system crashes without converging to the final answer. This problem is attributed to the circular cross sectional of the spiral coil wire since HFSS uses finite-elements analysis method which requires the object to be divided into thousands of tetrahedral segments. For a circular cross-sectional coil the number of these tetrahedral segments are too many, thus a long analysis time is required for one single coil. To avoid this problem, two approximations are made which don't have a significant effect on final result but reduce the analysis time considerably. The first approximation is to use spiral which is consisted of polygon loops instead of circular loops. The second approximation is using polygon cross-sectional area for coil wire instead of circular cross-sectional wire.

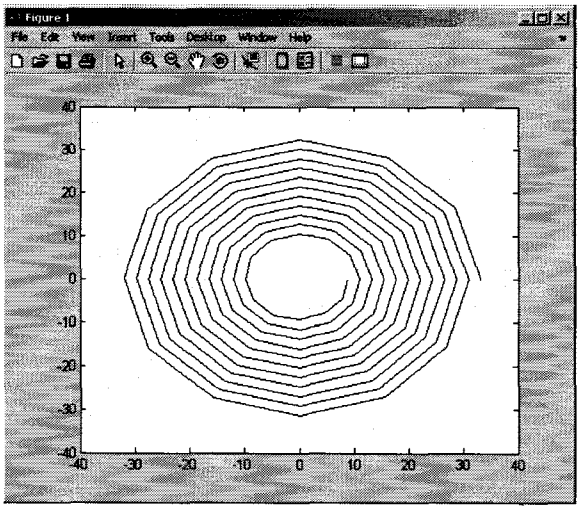

Figure 3.2 Spiral path of a polygon produced by MATLAB

Unfortunately HFSS does not have a straight method for producing a polygon coil with polygon cross-sectional wire. To produce this type of coil one can resort to other options in this software for this purpose. For example it can extrude any drawn polygon along a defined path to produce a geometrical design. This option is used

here to produce the desired approximated coil. HFSS can not produce a polygonal spiral path, thus this path is produced here with a MATLAB program (Figure 3.2) and again through MATLAB programming the produced coordinates are transformed to a DXF format file which is the only way a path file can be imported by HFSS.

Here a hexagon is drawn as the cross section of the coil wire which is later on extruded along the imported spiral path to produce the desired approximated coil (Figure 3.3). The analysis time of this approximated coil is significantly reduced which allows one to analyze different coil shapes (i.e. for different winding pitch) in a very short time.

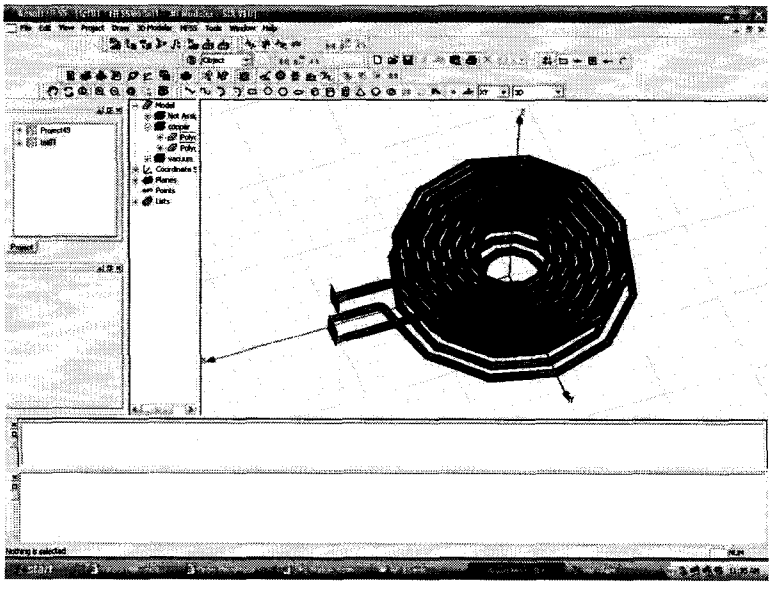

Figure 3.3 Extruded spiral path produced by MATLAB in HFSS environment

Using this method a pancake shape transcutaneous transformer for the coils diameter of 8 cm is designed. Several coils with different turning loops and winding pitches are assumed and accordingly their corresponding structures are created with the method just described. Eventually it turned out that the coils with winding turns

of 16 whose winding pitch is 4 mm gives the best coupling for this particular coil sizes. The self-inductance of each of these coils are $12\mu H$ and the mutual-inductance of them is $2.5\mu H$ for a separation distance of 15 mm.

3.3 Transcutaneous Transformer Electrical Model Determination

When the coils are designed and wound, through some measurements the elements of the transcutaneous transformer can be calculated. In this section it will be shown that by measuring the inductance of each side while the other side is either short circuited or open circuited, the primary and secondary leakage inductances and also the coupling inductance can be calculated.

We assume that the number of primary and secondary winding turns in the ideal transformer of Figure 2.3 which represents an electrical circuit for the transcutaneous transformer are the same. By short circuiting the secondary side of this figure and transferring all the elements of the secondary side to the primary side (Figure 3.4), the equivalent inductance seen from the primary side is:

$$L_{PSC} = LL1 + LM||LL2 \tag{3.1}$$

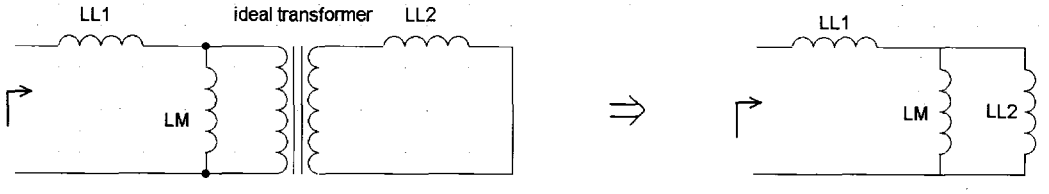

Figure 3.4 Impedance seen from primary when secondary is short circuited in a transcutaneous energy transfer system electrical circuit

In the same way, by leaving the secondary open circuit, the inductance seen from primary side (Figure 3.5) would be:

$$L_{POC} = LL1 + LM \tag{3.2}$$

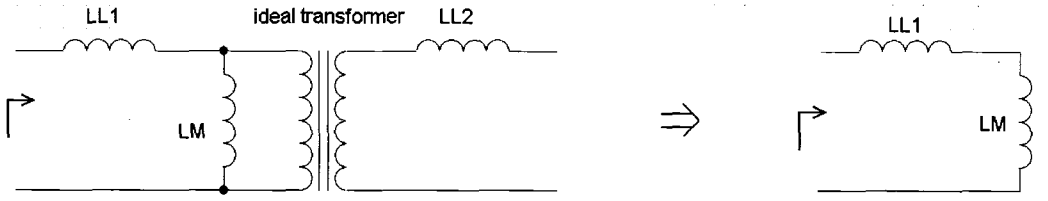

Figure 3.5 Impedance seen from primary when secondary is open circuited in a transcutaneous energy transfer system electrical circuit

To determine the values of LL1, LL2 and LM, the elements of the electrical model of the transcutaneous transformer, one more equation would be needed. This equation can be found by either short circuiting or leaving the primary side open circuit and measuring the secondary inductance. Let's leave the primary side open circuit and measure the inductance seen from secondary side (Figure 3.6). This inductance would be:

$$L_{SOC} = LL2 + LM \tag{3.3}$$

By simultaneously solving the set of equations of (3.1), (3.2) and (3.3), the values of LL1, LL2 and LM could be derived, resulting in the following equations:

$$LM = \sqrt{L_{POC} * (L_{POC} - L_{PSC})} \tag{3.4}$$

$$LL1 = L_{POC} - L_M \tag{3.5}$$

$$LL2 = L_{SOC} - L_M \tag{3.6}$$

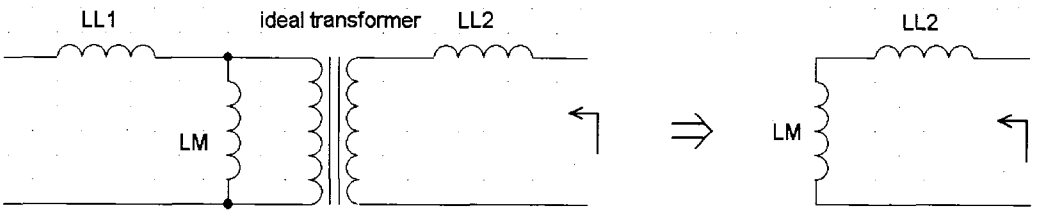

Figure 3.6 Impedance seen from secondary when primary is open circuited in a transcutaneous energy transfer system electrical circuit

Chapter 4

CLASS-E COIL-DRIVER

In this work the Class-E amplifier is used to drive current into the primary coil of a transcutaneous transformer. Before going into details of this particular design in the following chapters, a brief introduction to operation theory, analysis and design of the Class-E amplifier and rectifier is given here.

4.1 Class-E Amplifier

The Class-E amplifier was introduced by Sokal [16] in 1975. This amplifier, when designed properly, has a theoretical efficiency of 100% which is mainly due to zero switching losses of its switching transistor. This amplifier is also safe against load short circuit, has very simple structure and capability of working at high frequency [17].

The Class-E amplifier consists of a load network and a single transistor that is operating at the carrier frequency of the output signal (Figure 4.2).

4.1.1 Class-E Amplifier Definition

The definition of Class-E operation by Sokal [16] states three main objectives for the voltage and current waveforms of a switching transistor(Figure 4.1):

1. The rise of the voltage across the transistor at turn-off should be delayed until after the transistor is off.

2. The transistor voltage should return to zero before the transistor current begins to rise.

3. The slope of the transistor voltage should be zero at the time of turn-on.

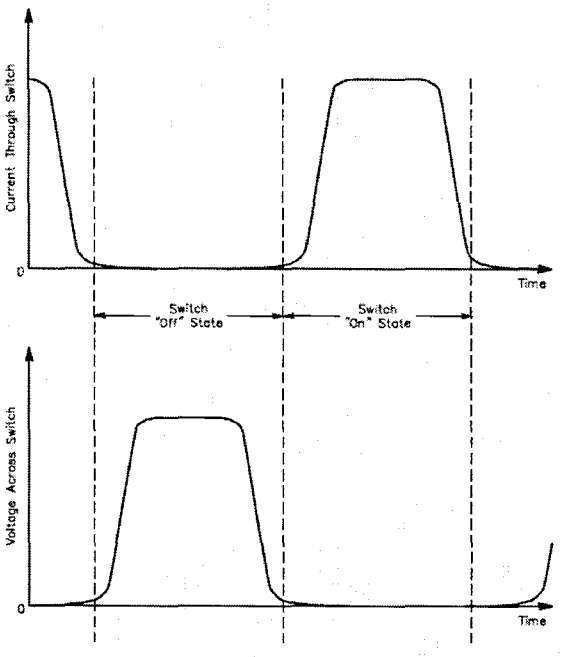

Figure 4.1 Ideal switch waveforms in a Class-E amplifier [16]

The first condition assures that high voltage does not exist across transistor while the current through it is nonzero, thereby avoiding the energy loss that would have

otherwise existed. The second condition states that while the transistor is off, the transient voltage across it first goes upward and then downward toward zero. This voltage should reach zero before the start of an "on" state. The third condition states that when the off state transient response reaches zero voltage across the switch, i.e., just before the start of the "on" state, it does so with zero slope which allows accidental slight mistuning of the amplifier without sever loss of efficiency.

4.1.2 Principle of Operation

Every amplifier that meets the definitions of a Class-E amplifier, provided in the previous section, is considered to be a Class-E amplifier. Figure 4.2 shows the most popular circuit used for a Class-E amplifier.

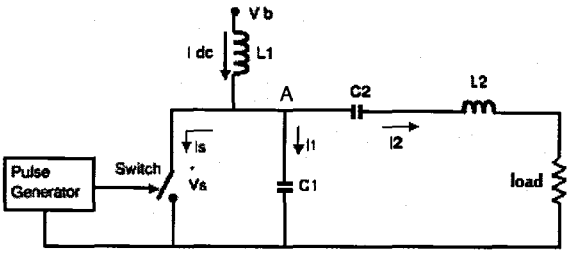

Figure 4.2 A Class-E amplifier

In this circuit it is assumed that the inductance of inductor L1 is so high that it can be considered to perform like a current source supplying the energy lost during circuit operation. It is also assumed that the tuned load network consisting of capacitor C2, inductor L2 and the load have a very high Q so that the current flowing through this network can be considered pure sinusoidal. This current flows through the switch when it is on. When the switch turns off this current keeps flowing but this time

through the capacitor C1, raising the voltage across it as well as across the switch. When the direction of the current is reversed, capacitor C1 starts supplying this current, reducing the voltage across it. The value for the C1 capacitor and the load network series resonant network elements can be designed to make this voltage not only reach zero but also have a zero slope at this instant. This instant is the best time for the switch to turn on since it allows current flowing through it while the voltage and also the slope of voltage across it is zero which makes the energy loss during the switching period almost zero. The zero voltage is required for a zero switching loss operation while the zero slope prevents a slight timing error to have a significant effect on transistor switching losses.

4.1.3 Analysis

Although there are other methods for analyzing a Class-E amplifier such as the analysis method presented by Puczko et. al. [22], in this thesis the method introduced by Raab [23] is chosen for analyzing the Class-E coil-driver of the transcutaneous energy transfer system. This method is accurate and simple, as compared to the other methods, and is more referenced by other works [27]. In this method it is assumed that the quality factor (Q) of the series resonant load network is high enough so that the current flowing through it is sinusoidal. Figure 4.3 shows the waveforms of the transistor driving voltage, the load voltage, the voltage across the transistor and the current flowing through the transistor. The voltage and the current of the load are as follows:

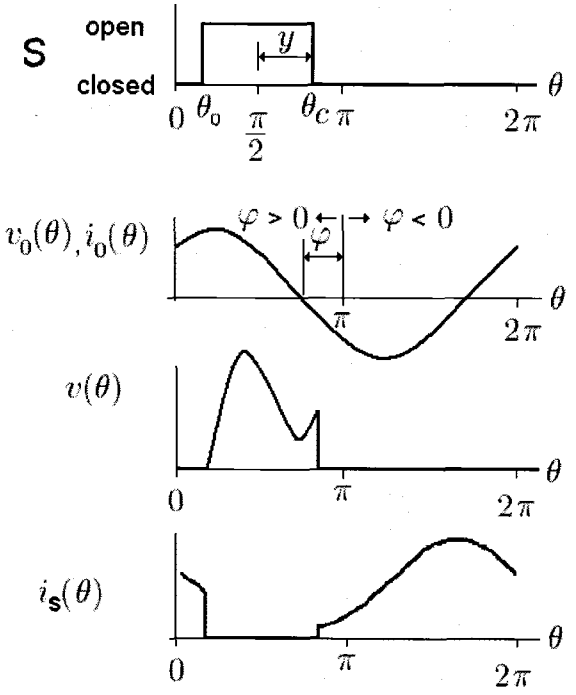

Figure 4.3 The switch driving signal, output voltage, switch voltage and switch current waveforms of a general Class-E amplifier [23]

$$v_0(\theta) = csin(\omega t + \varphi) = csin(\theta + \varphi) \tag{4.1}$$

$$i_0(\theta) = \frac{c}{R}sin(\omega t + \varphi) = \frac{c}{R}sin(\theta + \varphi) \tag{4.2}$$

Where:

$$\theta = \omega t \tag{4.3}$$

And the parameter "φ" is the phase angle which is defined in Figure 4.3. The objective of this analysis is to find "c" and "φ".

By assuming that the the transistor switch if off, the voltage at point A is a hypothetical voltage equal to:

$$v_1(\theta) = v_0(\theta) + v_X(\theta) = csin(\omega t + \varphi) + X\frac{c}{R}sin(\theta + \varphi) = c_1 sin(\omega t + \varphi_1) \tag{4.4}$$

Where X is the equivalent reactance of the series resonant network, L_2C_2, and:

$$c_1 = c\sqrt{1 + \frac{X^2}{R^2}} = \rho c \tag{4.5}$$

and

$$\varphi_1 = \varphi + \psi = \varphi + \tan^{-1}(\frac{X}{R}) \tag{4.6}$$

and ψ is the phase difference which is made by the series resonant network, L_2C_2:

$$\psi = \tan^{-1}(\frac{X}{R}) \tag{4.7}$$

The current flowing through capacitor C1, when the switch is off, is provided by the difference of the current of RF chock, L1, and the current of the series resonant network. The switch voltage is the voltage across capacitor C1 which is charged by this difference current, hence,

$$v(\theta) = \frac{1}{\omega c}\int_{\theta_0}^{\theta} i_c(u)du = \frac{1}{B}\int_{\pi/2-y}^{\theta}[I - \frac{c}{R}sin(u+\varphi)]du \tag{4.8}$$

where

$$B = \omega c \tag{4.9}$$

The fundamental frequency component of the switch voltage (C1 capacitance voltage) should be equal to $v_1(\theta)$ which is derived in (4.4). Thus c_1 would be the sinusoidal Fourier integral of (4.8). When the integrations are performed and the appropriate substitutions are made, then by collecting terms it would be possible to solve for "c" which is shown in (4.10)

$$c = IR\frac{2y\sin y\cos\varphi_1 + (2y\cos y - 2\sin y)\sin\varphi_1}{\pi BR\rho + \frac{1}{2}\sin(2\varphi+\psi)\sin 2y - y\sin\psi + 2\sin(y-\varphi)\cos\varphi_1\sin y} \tag{4.10}$$

$$= IRh(\varphi,\psi,y,B,R,\rho) \tag{4.11}$$

Still this equation is unable to determine the amplitude "c" since φ is unknown. Since the fundamental frequency component of the switch voltage, $v(\theta)$, is by definition a sinewave of phase φ_1, as stated in (4.4), there can be no cosine or quadrature component with respect to φ_1, thus a second relationship among the parameters, based on the fact that the cosine Fourier integral is zero, would be:

$$0 = \frac{1}{\pi}\int_0^{2\pi} v(\theta)\cos(\theta+\varphi_1)d\theta \tag{4.12}$$

By solving this equation the following result will be obtained,

$$c = IR\frac{2y\sin\varphi_1\sin y - 2y\cos\varphi_1\cos y + 2\cos\varphi_1\sin y}{-2\sin(\varphi-y)\sin y\sin\varphi_1 - \frac{1}{2}\sin 2y\cos(2\varphi+\psi) + y\cos\psi} = IRg(\varphi,\psi,y) \tag{4.13}$$

The similarities of equations (4.10) and (4.13) require that,

$$g(\varphi,\psi,y) = h(\varphi,\psi,y,B,R,\rho) \tag{4.14}$$

From this equation a value for φ can be found and accordingly the amplitude will be determined.

4.1.4 Design Procedure

To design a Class-E amplifier one should consider that there are two conditions that a Class-E amplifier should meet. The voltage and the voltage slope across the switch at turn on time must be zero. By applying these conditions, respectively, the following equations will result,

$$v(\theta)|_{\theta=\pi/2+y} \Longrightarrow g = \frac{y}{\cos\varphi \sin y} \tag{4.15}$$

$$\frac{dv(\theta)}{d\theta} = 0 \Longrightarrow \varphi = \tan^{-1}\left(\frac{y\cos y - \sin y}{y \sin y}\right) \tag{4.16}$$

Load Angle Determination

For designing a Class-E amplifier, one can find the load phase angle from equation (4.16). The resultant value, when plugged into (4.15), gives the value for "g".

Load Resistance Determination

The resistance that the amplifier shows to the power supply can be obtained by,

$$R_{dc} = \frac{V_{cc}^2}{P_o} \tag{4.17}$$

Where P_o is the output power and V_{cc} is the power supply voltage. The supply current would become

$$I = \frac{V_{cc}}{R_{dc}} \tag{4.18}$$

By considering that the output power is,

$$P_o = \frac{1}{2}\frac{c^2}{R} \tag{4.19}$$

And by involvement of (4.13), (4.15) and (4.16), the load resistance can be obtained

$$R = \frac{I^2 g^2 P_o}{2} \tag{4.20}$$

Series Resonant Tank Elements

By recalling (4.13)

$$g = \frac{2y \sin\varphi_1 \sin y - 2y \cos\varphi_1 \cos y + 2\cos\varphi_1 \sin y}{-2\sin(\varphi - y)\sin y \sin\varphi_1 - \frac{1}{2}\sin 2y \cos(2\varphi + \psi) + y\cos\psi} \tag{4.21}$$

The only unknown in this equation is the load phase angle which appears as $\varphi_1 = \psi + \varphi$. To determine ψ it is necessary to expand the term containing φ_1 so that $\sin\psi$ and $\cos\psi$ can be separated. This results in the following set of equations,

$$\tan\psi = \frac{q_1 \sin\varphi + q_2 \cos\varphi + q_3 \cos 2\varphi + gy}{q_2 \sin\varphi + q_3 \sin 2\varphi - q_1 \cos\varphi} \tag{4.22}$$

where

$$q_1 = -2g\sin(\varphi - y)\sin y - 2y\sin y \tag{4.23}$$

$$q_2 = 2y\cos y - 2\sin y \tag{4.24}$$

$$q_3 = -\frac{g}{2}\sin 2y \tag{4.25}$$

Once ψ is determined, one can use the following equation to find the reactance of the series resonant network from which the values of C2 and L2 can be easily determined.

$$X = R\tan\psi \tag{4.26}$$

Parallel Capacitor Determination

From (4.8) one can derive the following equation which can be employed to find C1, the parallel capacitor.

$$B = \omega C = \frac{2y^2 + 2yg\sin(\varphi - y) - 2g\sin\varphi\sin y}{\pi g^2 R} \tag{4.27}$$

Practical Adjustments

Once all component values are determined, through the design equations just derived, one can use Figure 4.4 [28] for the final fine tuning and adjustments.

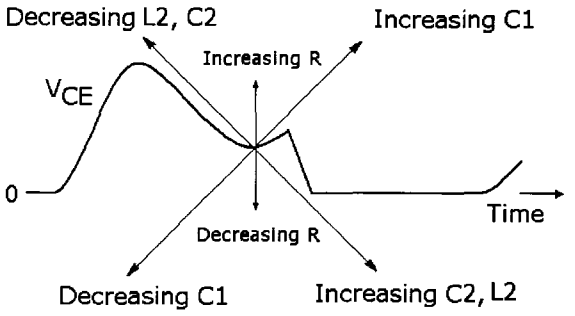

Figure 4.4 Final fine tuning of a Class-E amplifier [16]

For example in this figure the valley on the right lower side should touch zero-voltage line at the end of the "off" switching cycle. To do so both or either of L_2 or C_2 should be increased.

4.2 Load Variation Effects

Figures 4.5, 4.6 and 4.7 are obtained by simulating a Class-E amplifier working at Class-E operation point in this thesis. From Figure 4.5 it is seen that at the optimum load, the voltage across the transistor and also the slope of that voltage at switching

instant are both zero, allowing for zero voltage switching and slight timing error in transistor switching respectively.

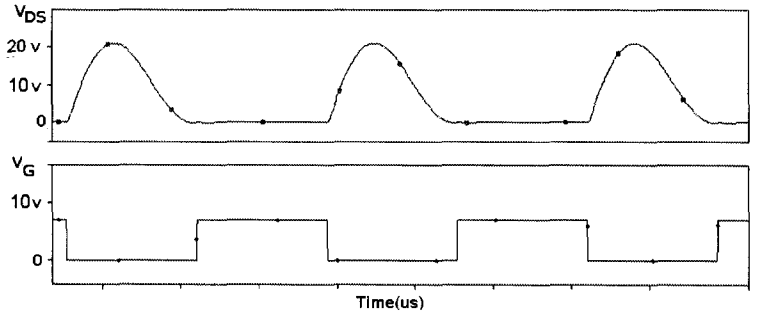

Figure 4.5 The Drain-Source and Gate voltage of the switching transistor of a Class-E amplifier when load resistance equal to optimum load

Figure 4.6 shows that as soon as the load resistance is increased from the optimum value, the parallel capacitor can not be completely discharged any more and neither zero voltage condition nor zero slope voltage condition across the switch will be maintained and consequently switching losses start to increase dramatically. Figure 4.7

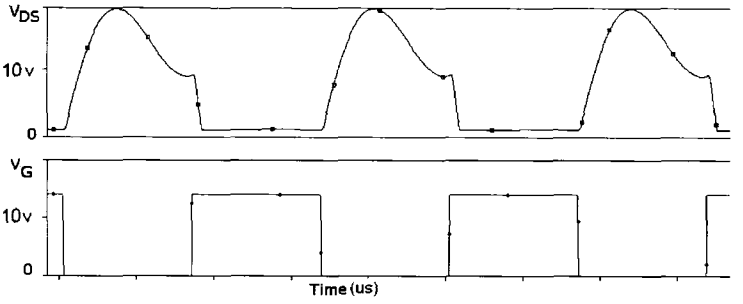

Figure 4.6 The Drain-Source and Gate voltage of the switching transistor of a Class-E amplifier when load resistance is larger that optimum load

shows the condition in which the load resistance is decreased from the optimum value. At this state the parallel capacitor discharges earlier than the instant the switch transistor turns on and hence the sine-wave current flowing through the series resonant

network will be supplied by the switch MOSFET transistor conducting in reverse direction. In case a bipolar transistor is used instead of a MOSFET transistor, an anti-parallel diode across transistor can maintain the same situation. In either of these cases the voltage across the switch transistor will remain zero (exactly as much as the voltage drop across a forward conducting diode is) and this ensures that the transistor will be turning on at zero voltage.

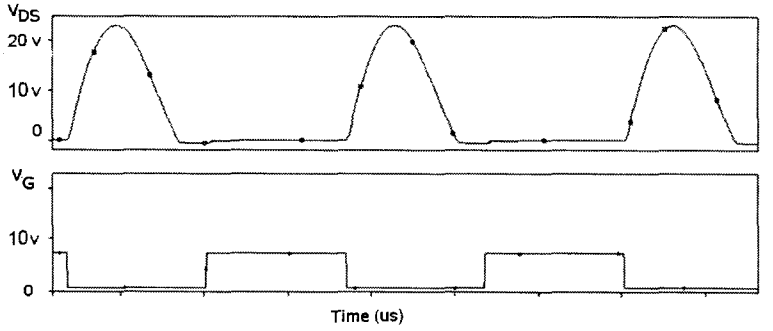

Figure 4.7 The Drain-Source and Gate voltage of the switching transistor of a Class-E amplifier when load resistance is smaller that optimum load

4.3 Class-E Rectifier

Class-E rectifiers offer a new means of high-frequency high-efficiency low-noise rectification [30]. Figure 4.8 shows a Class-E rectifier. It consists of a diode, a shunt capacitor and a second order low-pass output filter. The rectifier is driven by a sine-wave current source "i". The shunt capacitor shapes the voltage across the diode so that the diode turns on and off at low dv/dt, reducing the current driven through the diode at both transitions. The $L_f - C_f$ output filter ensures the ripple in the output voltage is below a specified level.

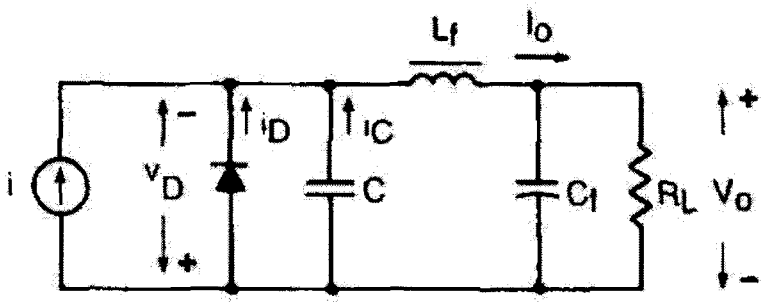

Figure 4.8 A Class-E rectifier [30]

4.3.1 Principle of Operation

The idealized current and voltage waveforms of the rectifier for the case where the diode on switch duty ratio is $D = 0.5$, i.e. when the conduction angle of the diode is equal to 180^o are shown in Figure 4.9.

The input current "i" of the circuit in Figure 4.9 is a sine-wave and the output current I_o is DC current. The diode and the parallel capacitor C are driven by a current source $I_o - i$. When the diode is off, the current $I_o - i$ flows through the capacitor C. When the diode is on, the current $I_o - i$ flows through the diode. The diode turns on when its voltage increases beyond the diode threshold voltage and it turns off when its forward current decreases to zero. The current flown through the capacitor C, when the diode is off, shapes the voltage across the diode. The relationship between the current and the voltage of a capacitor is $i_C = Cdv_D/dt$. This equation indicate that when the current flowing through the capacitor C is zero when the diode is turned off, the slope of the voltage across this capacitor, and hence the diode D which is placed in parallel with this capacitor, would be zero. On can follow through the waveforms of Figure 4.9 that the diode voltage at turn-off, v_D,

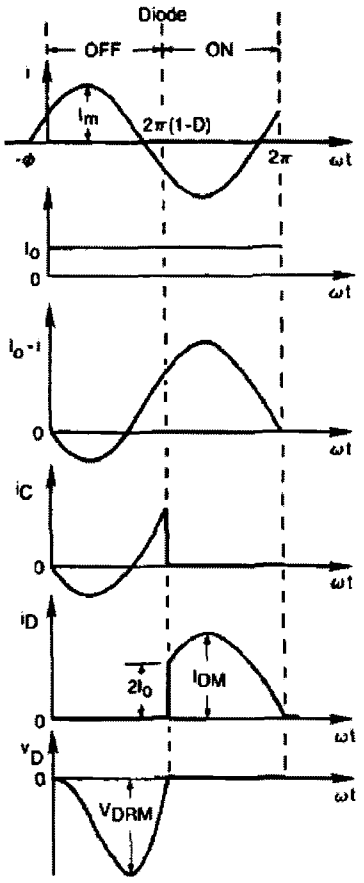

Figure 4.9 Idealized current and voltage waveforms of a Class-E rectifier [30]

gradually decreases when the capacitor current, i_C, is negative. This voltage reaches its minimum value when capacitor current is back to zero and then slowly rises when i_C turns positive. Thus diode turns on and off at low dv/dt, reducing switching losses as well as the switching noise. Moreover, the absolute value of diode current slope at turn on, which is equal to capacitor C current slope at this instant, is quite small since the diode voltage (Capacitor C voltage) at this instant is zero. This fact helps to alleviate the effect of reverse recovery charge of the diode.

4.3.2 Analysis

The basic equation for the rectifier of Figure 4.8 is:

$$I_o - i = i_D + i_C \tag{4.28}$$

In this equation,

$$i = I_m \sin(\omega t + \psi) \tag{4.29}$$

Where I_m is the amplitude and ψ is the phase angle indicated in Figure 4.9.

The relationship between the diode ON duty ratio D, and the phase angle ψ is given by [30],

$$\tan\psi = \frac{1 - \cos 2\pi D}{2\pi(1 - D) + \sin 2\pi D} \tag{4.30}$$

The diode on-duty cycle, D, depends on $\omega C R_L$ as follows,

$$\omega C R_L = \frac{1}{2\pi}\{1 - 2\pi^2(1 - D)^2 - \cos 2\pi D + \frac{[2\pi(1 - D) + \sin 2\pi D]^2}{1 - \cos 2\pi D}\} \tag{4.31}$$

For a particular operating frequency f and a diode turn-on duty cycle, D, the equivalent circuit for the Class-E rectifier is a series combination of resistor R_i and C_i capacitor. R_i is the input resistance of the rectifier and its value at the operating frequency ,$f = \omega/2\pi$, can be obtained by the following relation [30]:

$$R_i = 2R_L \sin^2\varphi \tag{4.32}$$

Where R_L is load resistance of the circuit. Likewise C_i is input capacitance of the rectifier whose value at the operating frequency, f, can be obtained by the following relation [30]:

$$C_i = C\pi[\pi(1-D)+\sin 2\pi D-\tfrac{1}{4}\sin 4\pi D\cos 2\psi-\tfrac{1}{2}\sin 2\psi\sin^2 2\pi D-2\pi(1-D)\sin\varphi$$

$$\sin(2\pi D-\varphi)]^{-1} \tag{4.33}$$

where C is the parallel capacitor of the Class-E rectifier.

Chapter 5

CLASS-E TRANSCUTANEOUS ENERGY TRANSFER SYSTEM

Compensating the effects of leakage inductances in a transcutaneous transformer helps to increase the voltage gain of a transcutaneous energy transfer system. These effects can be totally eliminated by employing resonant coil drivers such as Class-E or series resonant coils drivers, as were discussed in Chapter 2. Increasing the transcutaneous transformer coupling coefficient, as was discussed in Chapter 3, helps to reduce the leakage inductances and increase the efficiency of the system as well. However there are some other issues that should be considered in designing a transcutaneous energy transfer system. The fact is that, due to movement and breathing of the recipient of the implanted device, mutual position of two coils of the transcutaneous transformer is ever changing. These variations result in variation of coupling coefficient and leakage inductances of the transcutaneous transformer. Therefore, after the transcutaneous transformer is designed, not only its leakage inductances but also their variations for a specified interval, determined by the required mutual position

variation of the two coils, must be considered in the design. The other factors that must be considered in a good design are the prediction of load and input voltage variations. The control system employed for the design must also be capable to respond to these variations in a quick and effective way to ensure supplying of fixed and regulated voltage for the implanted device.

In this chapter the design method for a transcutaneous energy transfer system that is constructed for this thesis is outlined. The operation principles and the analysis method are first illustrated and then the potential capability of this system for keeping up with different coil positions and their effects on overall efficiency and operation frequency of the system are investigated.

5.1 Proposed Transcutaneous Energy Transfer System

Figure 5.1 shows the schematic diagram of the power transfer section of the proposed transcutaneous energy transfer system. In this system a Class-E amplifier is used as the coil-driver and a Class-E rectifier as the rectifier of the system. The primary leakage inductance of the transcutaneous transformer is playing the role of inductance in the tuned series network of the Class-E amplifier and effect of secondary leakage inductance is eliminated through resonance with the capacitor C3 at the operating frequency.

5.2 Circuit Analysis

To analyze the circuit of Figure 5.1 we start off by replacing the Class-E rectifier by its equivalent circuit which is a resistor in series with a capacitor as was outlined in Section 4.3.2. At this step the value for C_3 can be computed to make the two ca-

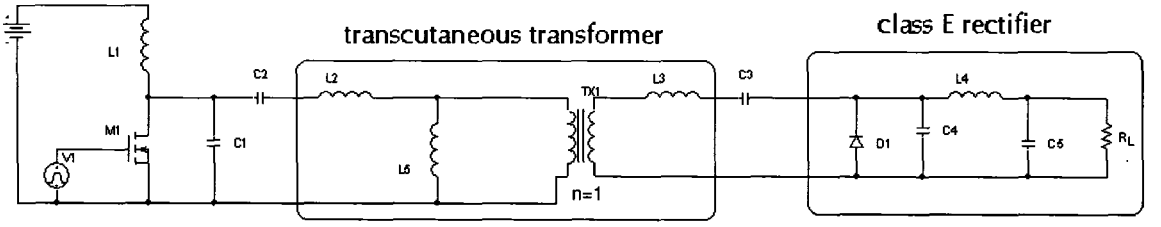

Figure 5.1 The schematic diagram of power transfer section of the proposed transcutaneous energy transfer system

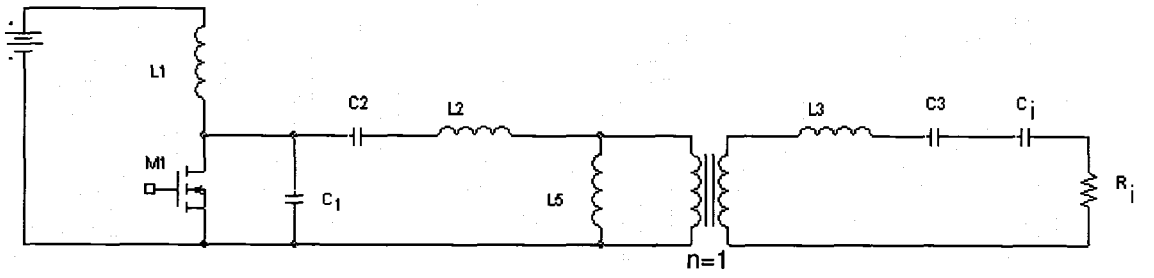

Figure 5.2 Figure 5.1 when its class-E rectifier is replaced by its equivalent circuit

pacitors C_3 and C_i and the secondary leakage inductance to resonate at the operating frequency to cancel out the secondary leakage inductance (Figure 5.3).

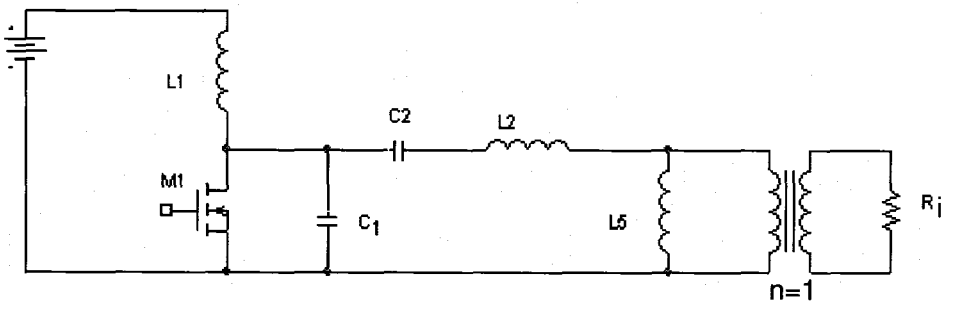

Figure 5.3 Figure 5.1 when the secondary leakage inductance is eliminated by resonance

After transferring R_i to the primary side, the circuit will change into Figure 5.4.

By transforming a parallel combination of a resistor and an inductor to a series

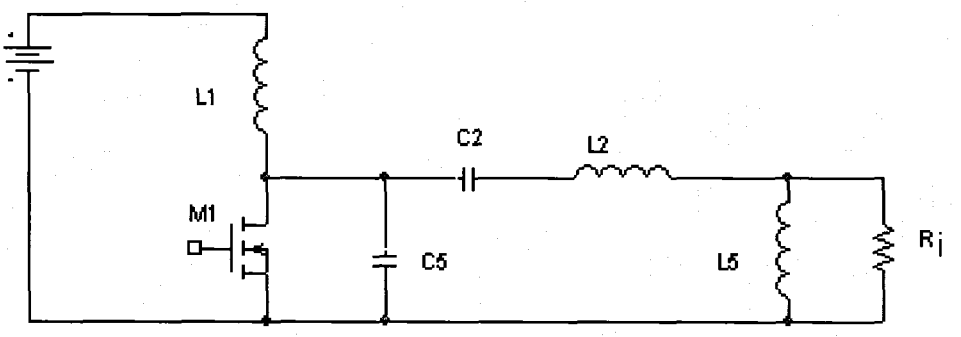

Figure 5.4 Figure 5.3 when secondary load is transfered to primary side

combination by appropriate equations [29] the circuit of Figure 5.5 will be the result.

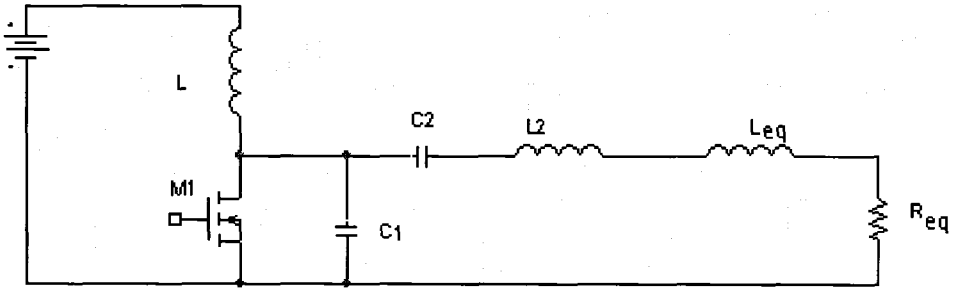

Figure 5.5 Figure 5.4 when parallel L_5 and R_i are replaced by their equivalent series combination

And finally it will reduce to the conventional form of a Class-E amplifier whose elements can be computed by the design method outlined in section 4.1.4.

5.3 Frequency Controlled Output Voltage

It would be very interesting to investigate the effect of operating frequency variation on output voltage variation. One would note that in this circuit the effect of the frequency variation is not limited to the series resonant network of the Class-E coil-driver. The secondary side tuned circuit which is used to eliminate the effect of

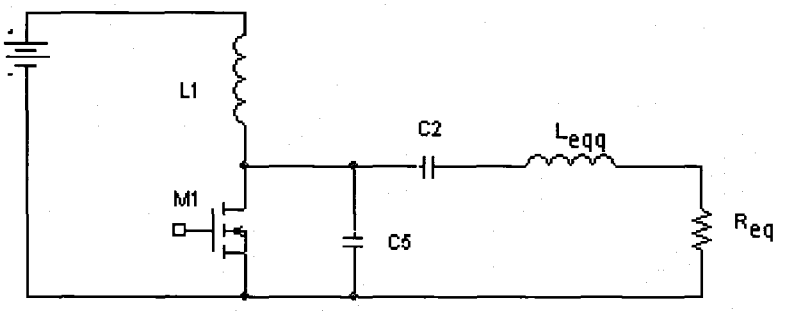

Figure 5.6 A Class-E amplifier

secondary side leakage inductance of the transcutaneous coils perform like another tuned filter in this circuit. Interaction of these two filters should be carefully studied to find potential operating conditions under which a linear and effective control over the output voltage would be possible .

5.3.1 Coils Coupling Variations Compensation by Frequency Variation

Any variation in mutual positions of the coils will change the coupling coefficient between them. This will lead to leakage and coupling inductances variations in the electrical transcutaneous transformer model and these in turn will result in resonance frequency variations of both of the filters. By increasing the distance between the two coils, their coupling decreases, their leakage inductances will be increased and the coupling inductance will be decreased. This will result in reduction of the resonant frequency in both of the filters. Thus intuitively decreasing the operating frequency can be accounted for compensating the coil distance increase. In the same way the increase in operating frequency can account for compensation of coils distance reduction. Hence frequency variation can reasonably be a means of compensating the coils mutual movements.

5.3.2 Load Variations Compensation by Frequency Variation

By assuming a fixed coils distance, variation of operation frequency in an allowed frequency band can also account for load variation in the allowed range the device is designed for. This can be visualized by assuming that when the load is varied, the Q of the Class-E amplifier will be varied. If it is assumed that the operating frequency band of the Class-E coil-driver is larger than its resonant frequency, i.e. it is situated at the right side of the center frequency in Figure 5.7, then by increase of the load, the voltage gain will be increased, thus a reduction in operating frequency is needed to compensate for this raise of load.

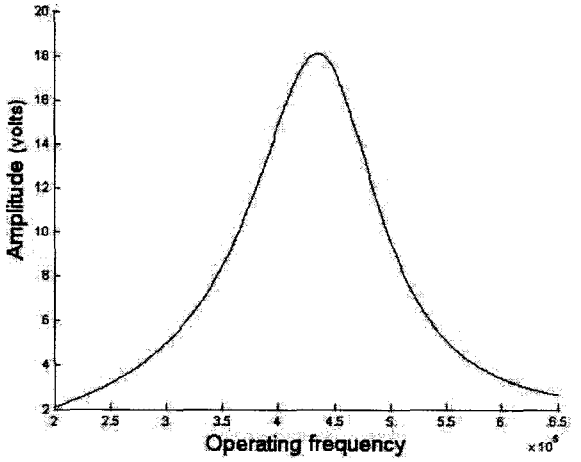

Figure 5.7 Frequency response of a Class-E amplifier

5.3.3 Frequency Variations Analysis

Studying the effects of frequency variation on the proposed circuit of Figure 5.1 is not a simple task since the role of the two tuned circuits should be considered at the same time. One approach to perform this analysis will be explained here. The circuit of Figure 5.3 when its series tuned circuit of the secondary side is replaced by

jX is shown in Figure 5.8.

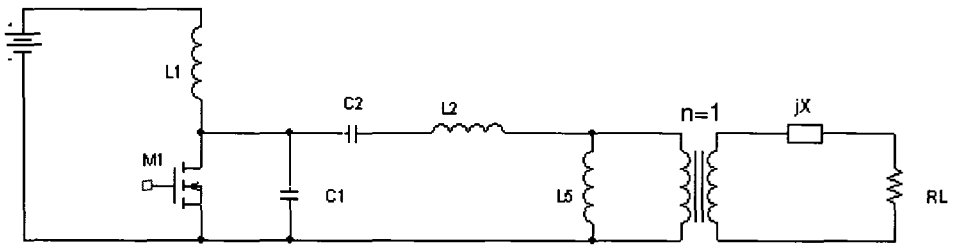

Figure 5.8 The Class-E transcutaneous energy transfer system with equivalent secondary side circuit

When the operating frequency is lower than the resonant frequency of the tuned filter, the X would change to a capacitance and when the frequency is higher than the resonant frequency, it will change to an inductance. For further processing the circuit on the secondary side will be transferred to the primary side as shown in Figure 5.9.

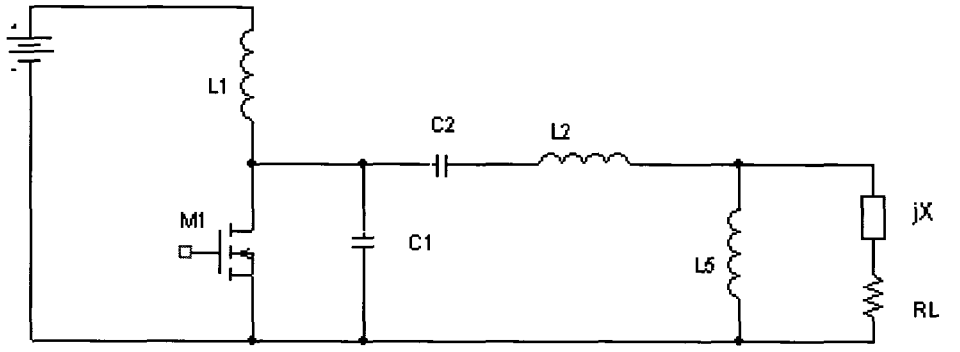

Figure 5.9 The Class-E transcutaneous energy transfer system with secondary impedance is transferred to primary side

To simplify the analysis, the series combination of R_L and jX will be transformed to a parallel combination with the following equations as shown in Figure 5.10.

$$R_p = R_L(1 + Q^2) \tag{5.1}$$

$$X_p = X(\frac{1+Q^2}{Q^2}) \tag{5.2}$$

$$Q = \frac{X}{R_L} \tag{5.3}$$

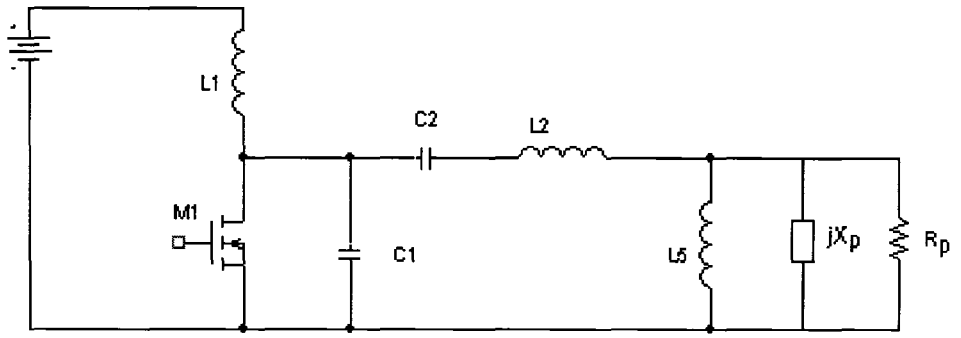

Figure 5.10 Figure 5.9 when series jX and R_L are transformed to parallel combination

jX and $j\omega L_5$ will be paralleled and the combination of the resulting inductance or capacitance and R_p will be transformed back to a series combination with the following equations (Figure 5.11)

$$R_s = R_p \frac{1}{(1+Q^2)} \tag{5.4}$$

$$X_s = X_p(\frac{Q^2}{1+Q^2}) \tag{5.5}$$

$$Q = \frac{R_p}{X_p} \tag{5.6}$$

The resulting circuit would be the conventional Class-E circuit which could be analyzed with the methods outlined in section 4.1.4

5.3.4 Frequency Response of the Proposed Transcutaneous Energy Transfer System

By utilizing the equations derived in the previous section the frequency response of the proposed transcutaneous energy transfer system can be computed. It will be

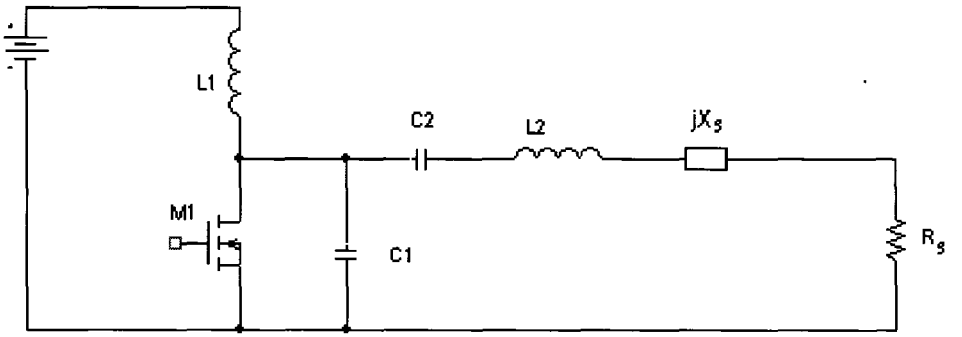

Figure 5.11 Figure 5.10 when parallel combination of reactance and resistor are transformed back to a series combination

shown that the overall frequency response which is the result of the interaction of the Class-E amplifier and the output tuned filter is more selective and narrow band than a Class-E amplifier by itself. In obtaining this frequency response, one also has some freedom to shape the frequency response of the overall system by choosing the location of the center frequency of the output tuned filter.

Frequency Response of a Class-E Amplifier

Figure 5.12 shows the frequency response of the Class-E amplifier which is obtained by mathematical modeling in MATLAB. This graph will be used as a reference to compare with and illustrate the frequency response of the complete transcutaneous energy transfer system.

Frequency Response of a Class-E Transcutaneous Energy Transfer System

Figure 5.13 shows the frequency response of the Class-E transcutaneous energy transfer system obtained by mathematical modeling in MATLAB. This graph is obtained while the secondary tuned circuit is fine tuned to the operating frequency for which the Class-E amplifier is designed. It can be seen that over part of the frequency

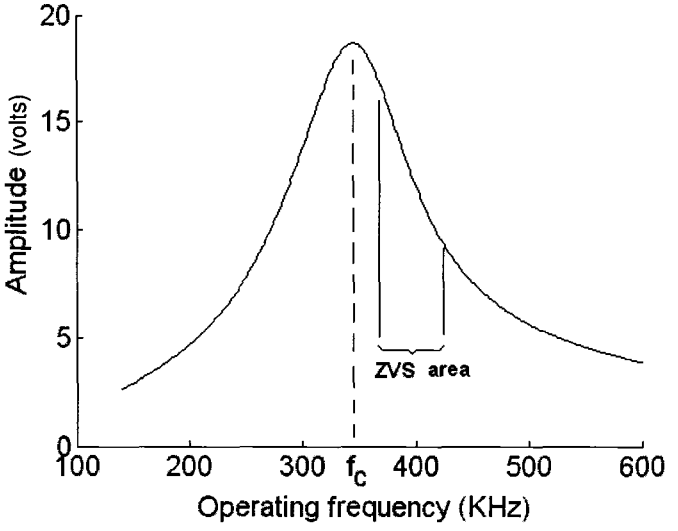

Figure 5.12 Frequency response of a Class-E amplifier

band the transfer function is obtained the voltage is fixed while over some other parts the output voltage is controllable by variation of the frequency. For controlling the output voltage also either of the left positive slope or the right negative slope could be used to control the output voltage. The control strategy and circuit limitations are among the factors which determine the working frequency band.

Figure 5.14 which is obtained by mathematical modeling by MATLAB, shows the frequency response of the Class-E transcutaneous energy transfer system when its secondary tuned circuit's resonant frequency is lower than the operating frequency for which the Class-E amplifier is designed. Definitely the larger peak is the most desired area for operation because of yielding better voltage gain for the system. Around this peak, depending on the control strategy and better linearity, either of the positive or negative slopes at the left or right side of the peak can be chosen.

When the secondary tuned circuit's resonant frequency is chosen to be higher than the operating frequency for which the amplifier is designed, the graph of Figure 5.15

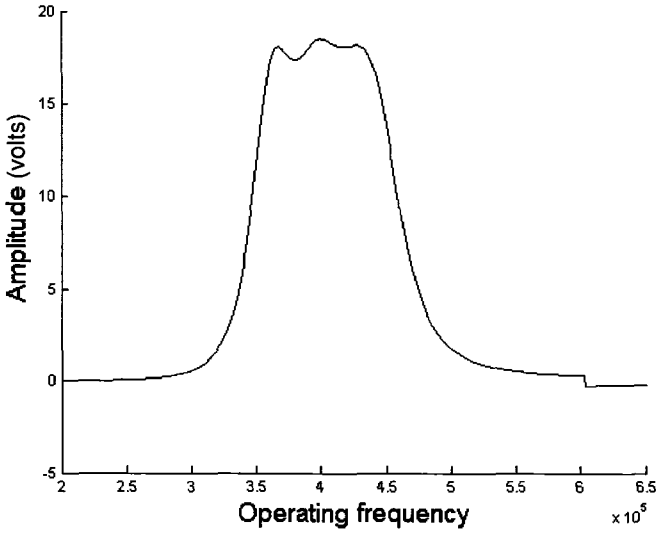

Figure 5.13 Frequency response of Class-E transcutaneous energy transfer system when f_{res} is very close to f_c

is obtained fron the mathematical modeling by MATLAB. This graph offers a number of options similar to those which already were discussed depending on which control region is selected.

In either of the three types of transfer function obtained, the Zero voltage switching (ZVS) condition has vital role in selection of the working frequency band since it directly influences the efficiency of the system. In all the three cases the zero voltage switching condition for Class-E amplifier switch are not investigated as it turned out the analysis procedure used doesn't have the potential for this investigation and thus this is left for further analysis and simulations to investigate the case which is performed in the next chapter.

Discussion

There is some discussion as what would be the potential benefits for a specific location of the resonant frequency of the secondary tuned filter. It is obvious that the

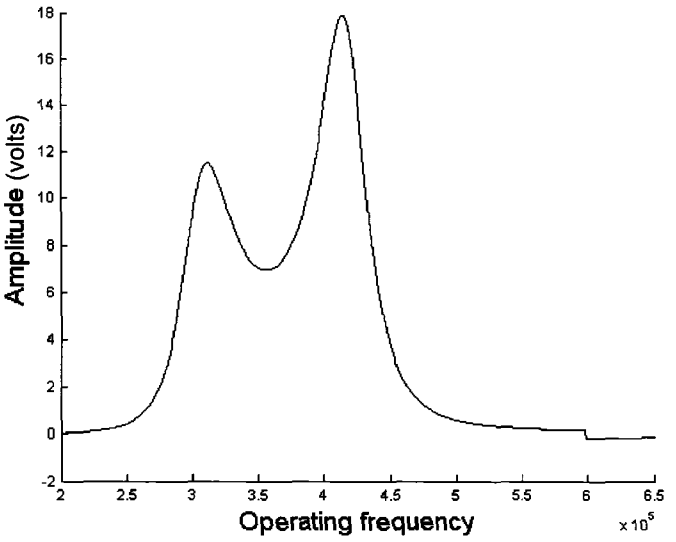

Figure 5.14 Frequency response of Class-E transcutaneous energy transfer system when f_{res} lags f_c

effect of the secondary side resonant filter is just resistive when its resonant frequency is equal to the operating frequency. If at this frequency the zero voltage switching state for the coil-driver is maintained then the peak corresponding to this filter in the transfer function of the transcutaneous energy transfer system is a safe region for operation, either it is smaller or greater than the peak corresponding to the Class-E coil-driver. But Figure 5.12 indicates that the safe operating area for a Class-E amplifier is at the right side of its peak frequency, thus depending on where the resonant frequency of the secondary filter is selected different situations may appear. First, assume it is smaller than the peak Class-E coil-driver frequency. In this case the area on the right skirt of Figure 5.14 is the useful operating area. The same situation occurs when these two frequencies are very close to one another. When the resonant frequency of the secondary resonant filter is larger than Class-E coil-driver peak frequency, either part or all of the positive or negative slope of each of the

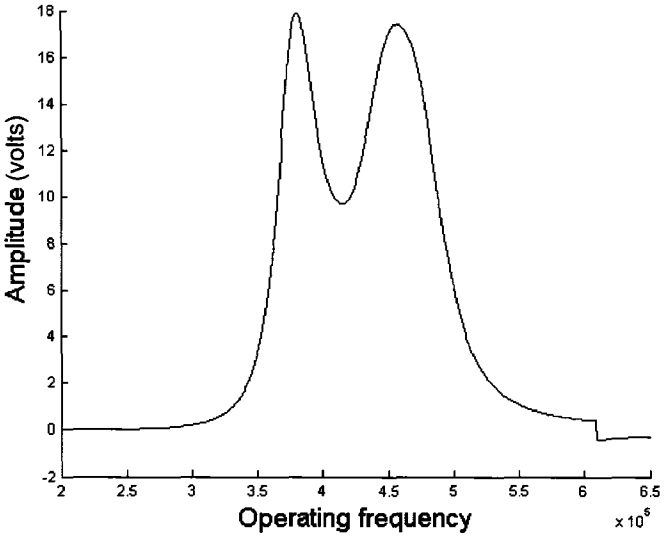

Figure 5.15 Frequency response of Class-E transcutaneous energy transfer system when f_{res} leads f_c

two peaks in the transfer function of Figure 5.15 might be a useful area for system operation. This gives some guidelines as how to obtain the desired transfer function by proper design. One can initiate the design by considering only the resistive effect of the secondary side on the primary and design the Class-E coil-driver and obtain its transfer function. By selecting the proper value for the secondary series capacitor, location of the secondary resonant filter on the Class-E coil-driver can be obtained.

Once the transcutaneous energy transfer system is designed and the control strategy is identified, a closed-loop stability analysis should be performed to avoid any oscillations due to instability which is the subject of the next section.

5.3.5 Closed-Loop Control and Stability Analysis

A closed-loop control technique is employed to keep the output voltage fixed and regulated by changing the operating frequency. Figure 5.16 shows the block diagram of this system.

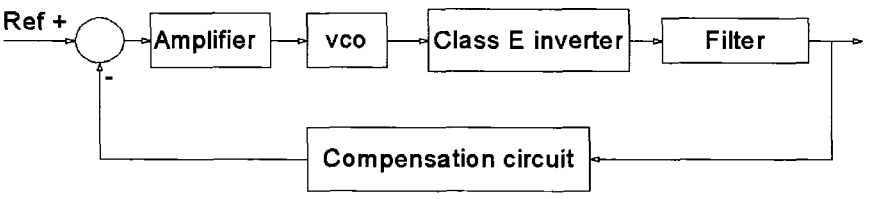

Figure 5.16 Block diagram of a closed-loop frequency controlled transcutaneous energy transfer system

The block "Class-E inverter" represents the Class-E amplifier, transcutaneous transformer and Class-E rectifier, excluding its output filter. As far as control analysis is concerned this block is assumed to have a linear transfer function for a limited band of frequencies for which the system is designed to operate. The output filter of the Class-E rectifier is a second order filter whose effect should be considered on the control loop. The output voltage is compared with a reference voltage whose result, after amplification, is used to produce the particular frequency needed for the required output voltage. As mentioned, except for the output filter which is frequency dependent and has a second order transfer function, every other block in the diagram has a fixed transfer function which would be represented by its gain value. A compensation circuit is required in the system to account for any instability that may occur in the operation of the system. To study the stability of the system, first the uncompensated system is modeled in Simulink as shown in Figure 5.17.

In this figure the difference amplifier and the VCO are represented by a constant value which is their combined gain. The second order output filter is represented by its transfer function which is shown in (5.7).

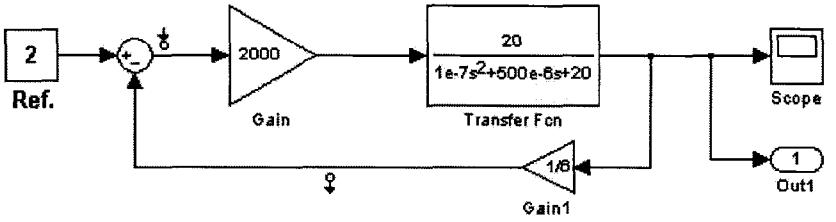

Figure 5.17 Modeling of the transcutaneous energy transfer system in the SIMULINK

$$H(s) = \frac{R_{out}}{(R_{out}CL)s^2 + Ls + R_{out}} \tag{5.7}$$

After analysis, the gain and phase plots of the system are obtained which are shown in Figure 5.18.

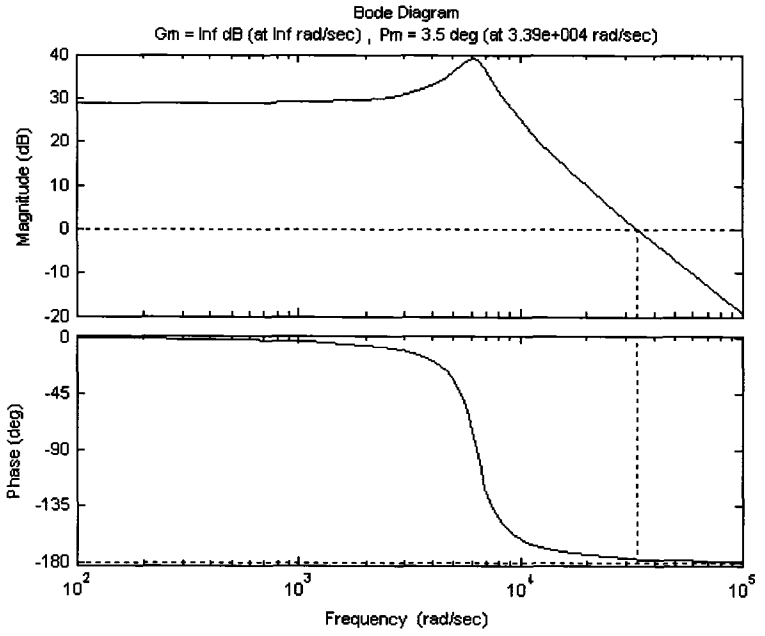

Figure 5.18 Gain and phase margins of the uncompensated transcutaneous energy transfer system

As it is seen the system in this state has very poor phase margin of 3.5^o thus it is very likely to oscillate. To prevent the system from oscillation and to avoid the unity

gain situation in the entire range of operating frequency band a compensation circuit is required to improve the phase margin of the system. Among different choices for the compensation circuit, a dominant pole circuit is used whose transfer function is represented by equation (5.8). Figure 5.19 shows the block diagram of the system after the compensation circuit is applied to it.

$$H(s) = \frac{1}{(R_{comp}C_{comp})s + 1} \tag{5.8}$$

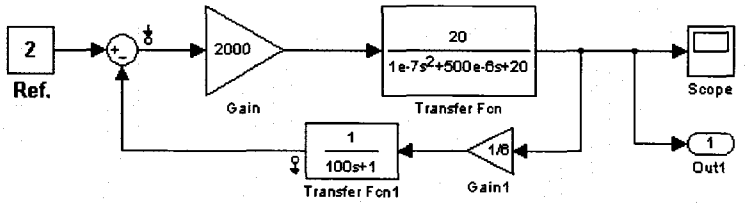

Figure 5.19 Modeling of the transcutaneous energy transfer system in the SIMULINK

The gain and phase plots of the compensated system are shown in Figure 5.20. These graphs indicate an improvement of up to $11.1dB$ and 90.4^o for gain and phase margins of the system respectively.

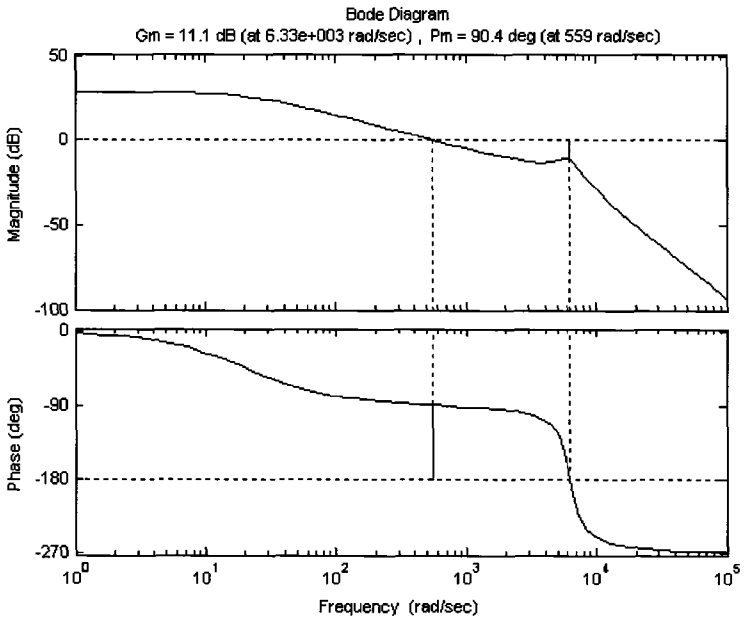

Figure 5.20 Gain and phase margins of the compensated transcutaneous energy transfer system

Chapter 6

SPICE SIMULATIONS AND EXPERIMENTAL RESULTS

To apply the methods outlined in the previous chapter a transcutaneous energy transfer system with the following specifications is designed:

- Input voltage 14 v
- Output voltage 12 v
- Maximum output power 15 W

It is assumed that the output voltage of this transcutaneous energy transfer system should be kept constant at the coils separation distances between 1 to 4 cm.

For this design no limitation on the size of the implanting coils is assumed. Based on the HFSS simulation, described in Section 3.2, each of the coils are wound with 16 turns of LITZ wire. According to the methods explained in Section 3.3 the elements of the electrical models of the transcutaneous transformer are determined through experimental measurements. This method could be used to obtain the curves of the leakage and the coupling inductances variation versus the coils separation distance.

The values of these inductances are limited to the coils extreme minimum and maximum separation distances the system is intended designed for. To start the design process, as the first step, the coupling and leakage inductances are obtained for the average separation distances of the two required extreme positions. At this condition, the difference between the values of the elements of the electrical models of the transcutaneous transformer, when the coils move to the each of extreme required position, is smaller than the case where initially these values are obtained for a different position than average of the two required extreme separation distance. In this way the chance of compensating the effects of variation of values of these elements by the variation of the operating frequency, which is the goal of this study, is increased.

Determination of other circuit elements such as Class-E rectifier and Class-E amplifier elements of Figure 5.1 are performed on the next step. This is performed according to the methods explained in the Chapter 4 whose MATLAB programs are already developed.

The circuit will then be simulated with PSPICE for a range of operating frequencies suggested by either of the graphs of Figures 5.13, 5.14 or 5.15. This is for finding the band of frequencies for which the output voltage is linearly controlled while ZVS is maintained. For example in this particular design, the transfer function depicted in Figure 6.1 is used.

It would be desirable to determine the ZVS property of region of interest directly by analysis than simulation since it would be much faster and more convenient. Unfortunately the basis of the analysis method used [23] doesn't seem to allow the analytical exploration of this option. However an indirect analysis is possible and

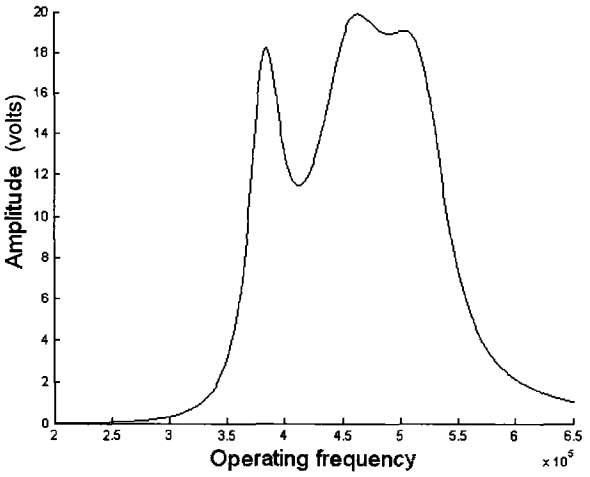

Figure 6.1 Frequency response of the analyzed 15 W, 12 v output Class-E transcutaneous energy transfer system

that is to check this region for ZVS property by observing the analyzed MOSFET drain voltage waveforms in MATLAB. The graphs depicted in Figure 6.2 are the waveforms obtained in this way for the range of operation frequencies form $360kHz$ to $440kHz$.

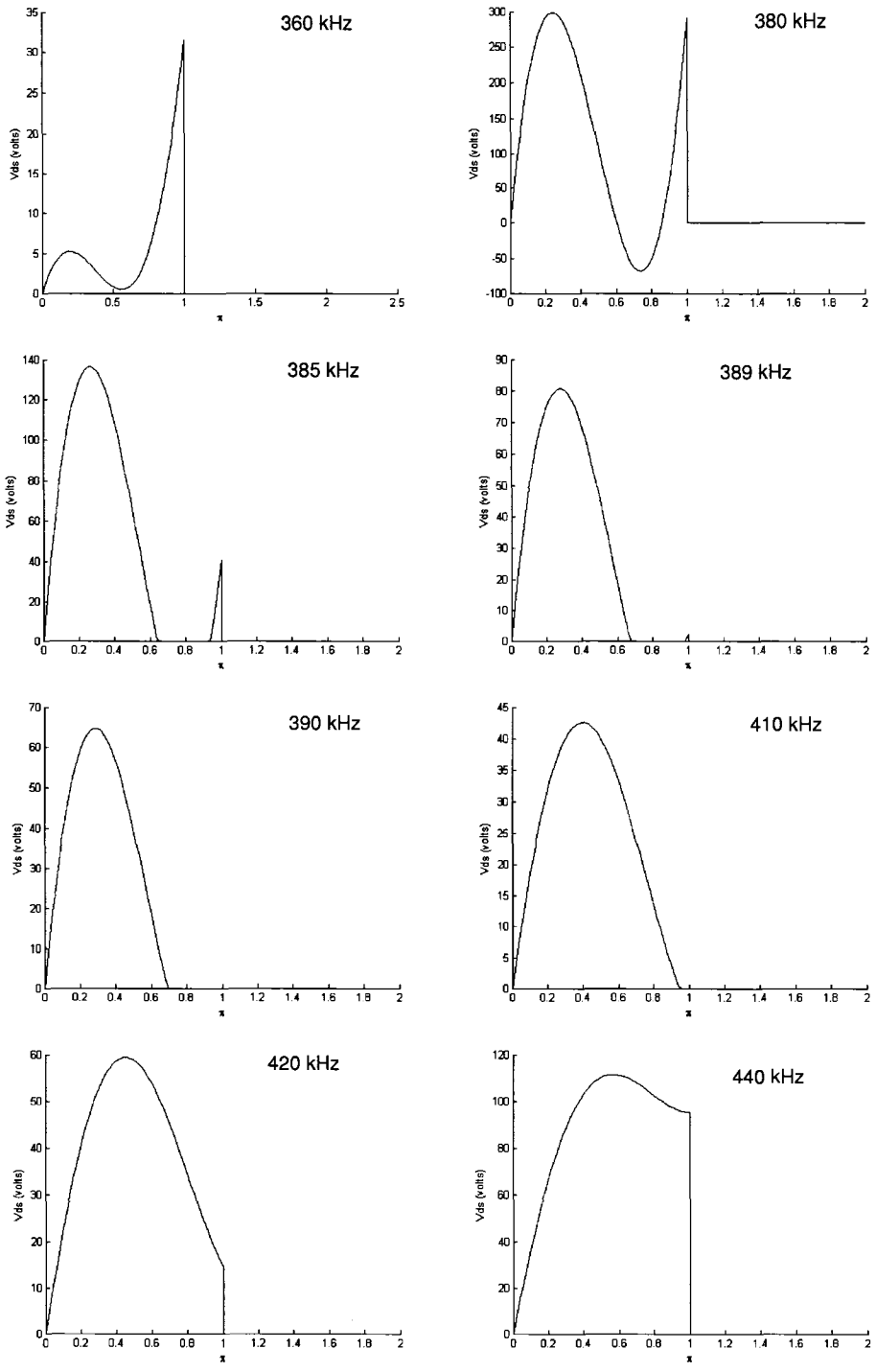

Figure 6.2 Drain waveform obtained by MATLAB from top left to the bottom right for the frequencies of $f_{op} = 360$kHz, $f_{op} = 380$kHz, $f_{op} = 385$kHz, $f_{op} = 389$kHz, $f_{op} = 390$kHz, $f_{op} = 410$kHz, $f_{op} = 420$kHz, $f_{op} = 440$kHz respectively

This figure indicates that at the frequency band between 389 kHz and 410 kHz, ZVS is maintained and this band is most likely the most suitable range for controlling the output voltage. To confirm this prediction, the designed transcutaneous energy transfer system may be simulated in SPICE at the selected frequency range to validate our initial prediction according to analytical waveforms obtained by MATLAB.

6.1 Simulations

6.1.1 Power Transfer Simulations

Figure 6.3 shows the circuit simulated in PSPICE.

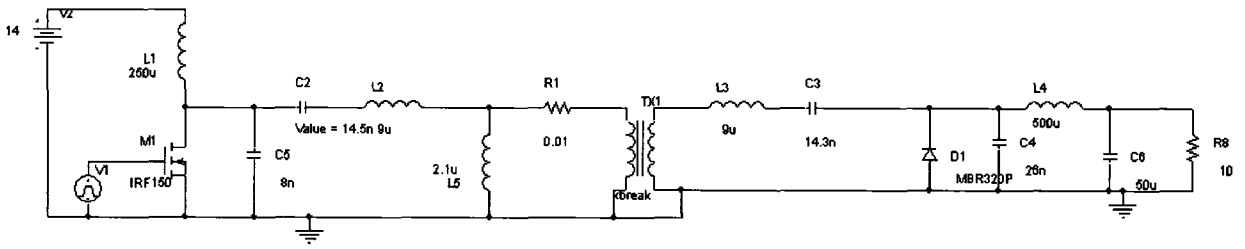

Figure 6.3 The power section of designed transcutaneous energy transfer system circuit modeled in SPICE. The connection between the grounds of the two sides of the transformer is necessary for simulation purpose.

Figures 6.5 to 6.7 demonstrate the MOSFET transistor voltage as well as the output DC voltage waveforms resulted from the SPICE simulations for frequencies from 350 kHz to 480 kHz. These waveforms confirm the results obtained by MATLAB in the previous section and indicate that the frequency range between 390 kHz to 410 kHz could be the suitable operating frequency band for controlling the output voltage in terms of maintaining the ZVS condition. These results also indicate that in the selected frequency band, the output voltage can be controlled between 15.7 v to 10.5 v which is obtained on the negative slope of the frequency transfer function shown if

Figure 6.4.

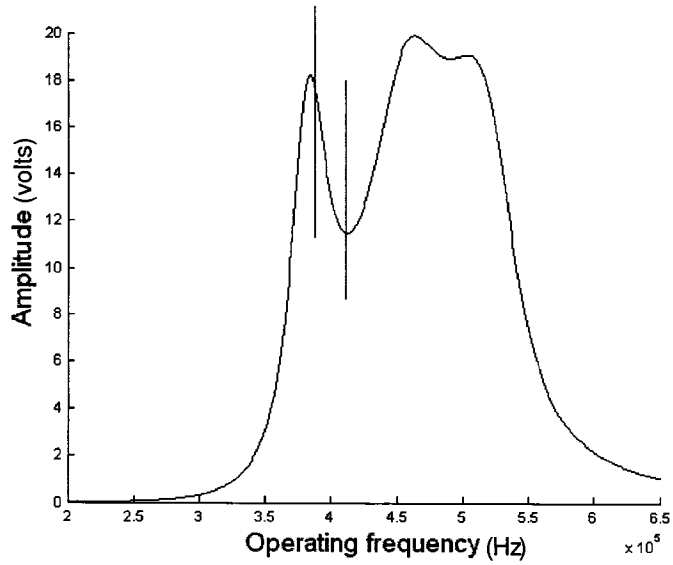

Figure 6.4 The portion of the transfer function between the two vertical lines is the area the system is working on

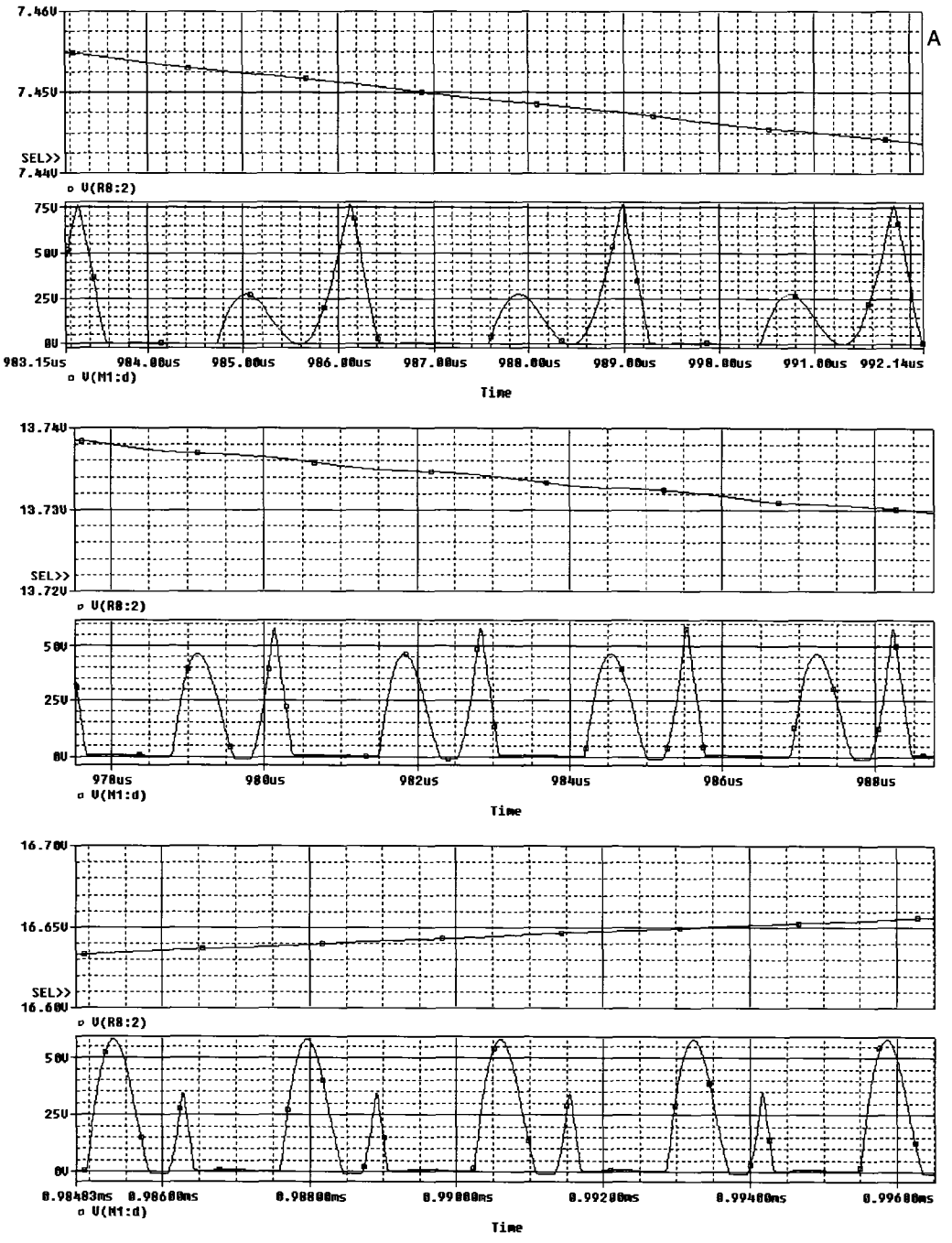

Figure 6.5 Simulated drain and output waveform at frequencies of f_{op} = 350 kHz, f_{op} = 370 kHz and f_{op} = 380 kHz from top respectively

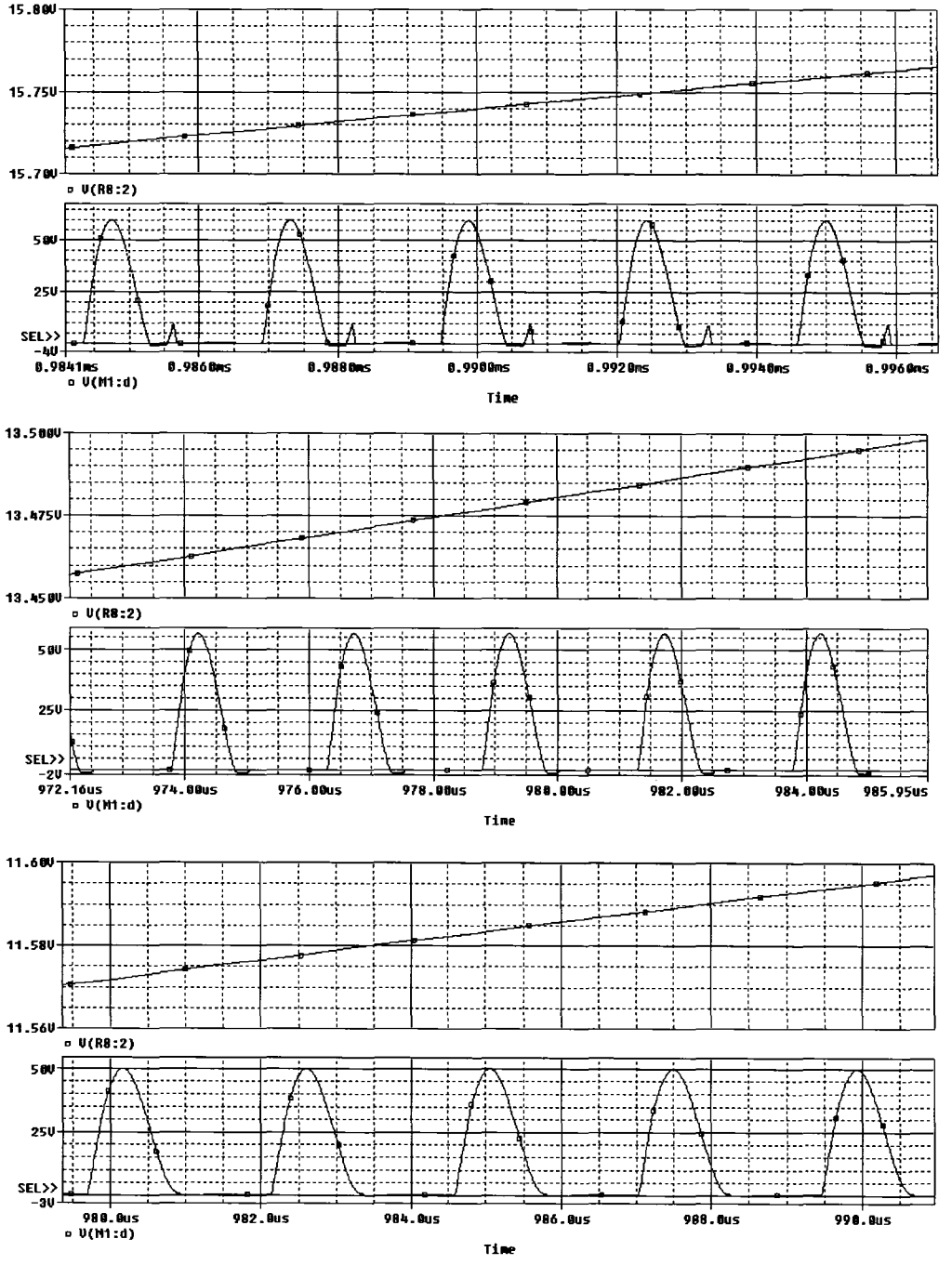

Figure 6.6 Simulated drain and output waveform at frequencies of f_{op} = 390 kHz, f_{op} = 400 kHz and f_{op} = 410 kHz from top respectively

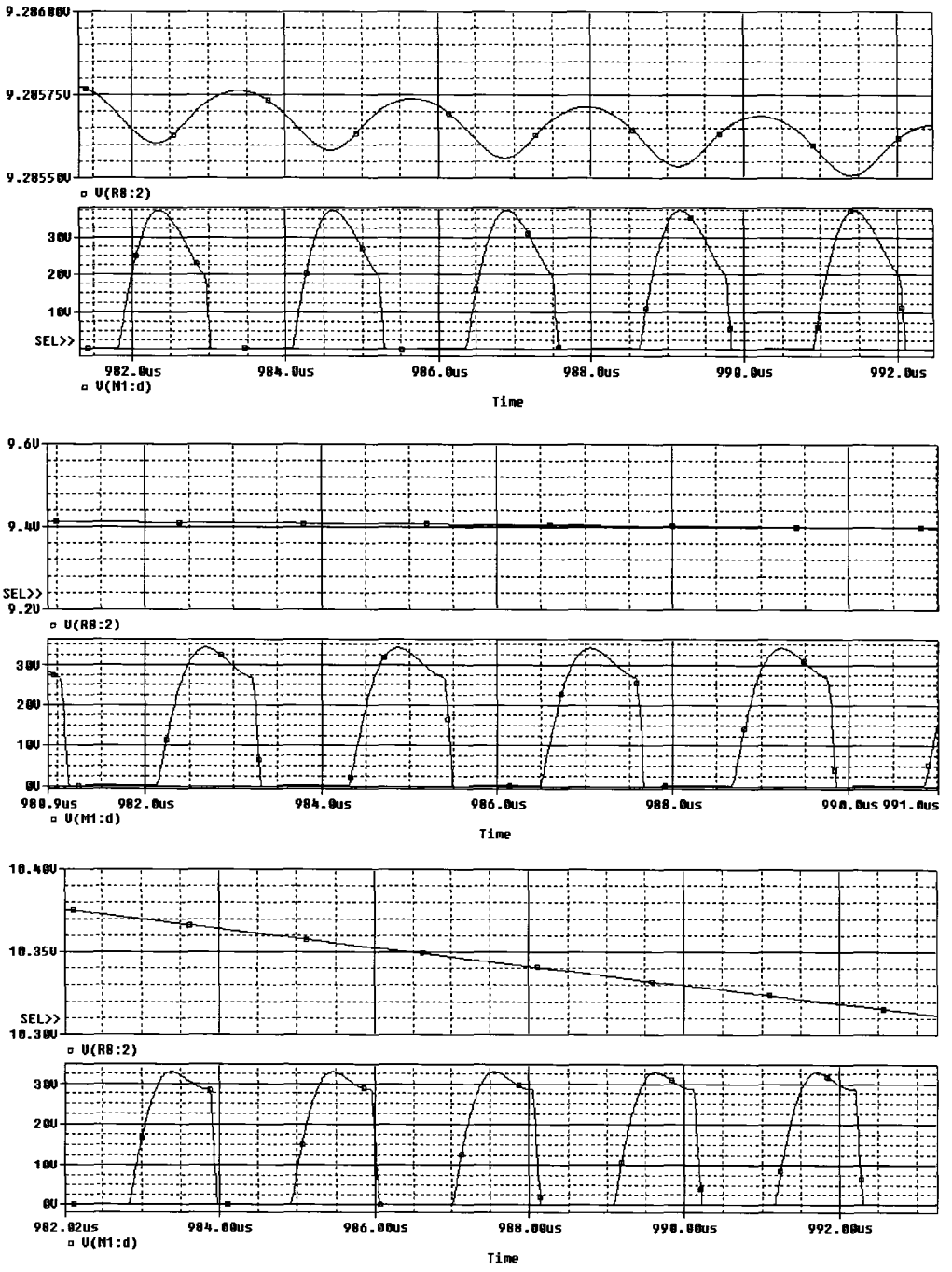

Figure 6.7 Simulated drain and output waveform at frequencies off_{op} = 440 kHz, f_{op} = 460 kHz and f_{op} = 480 kHz from top respectively

6.1.2 Closed-Loop Stability Simulation

In Section 5.3.5 an analysis was performed to determine the values of the components for the compensation circuit. Here, based on that analysis, the whole circuit is simulated to evaluate its performance with regard to stability.

Figure 6.8 shows the difference amplifier along with the compensation circuit which is composed of a proportional amplifier and an integrator. The difference of the sample of output voltage and a reference voltage, which is represented by a DC voltage source in spice simulation, is proportionally amplified by the amplifier of the first stage. The output of the first amplifier is integrated by the second stage amplifier in this figure.

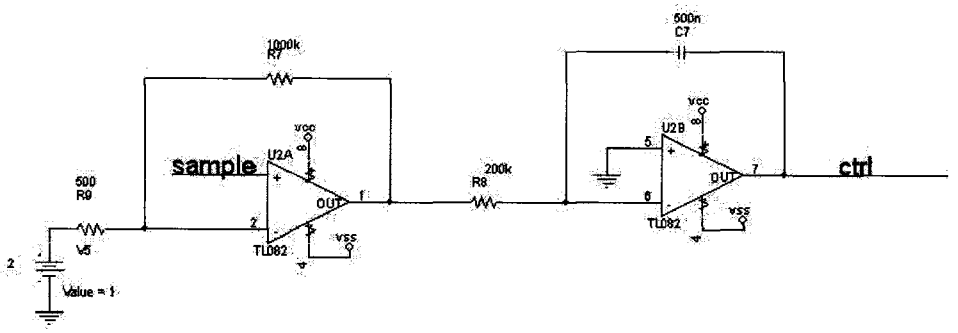

Figure 6.8 Proportional and integrator amplifiers in the closed control loop

The output of the integration amplifier is fed to a VCO behaviorally realized by the circuit of Figure 6.9. In this figure the capacitor C1 is charged by the behaviorial voltage-controlled current-source of G1 whose current is determined by the input control voltage, Vcont, and the input difference voltage. The input difference voltage is provided by the NAND Schmidt of U1A which oscillates between "0" and "5" volts. The voltage-controlled current source of G2 discharges the capacitor C1 with

the half amount of current G1 charges C1 when it is on. To describe the operation of this circuit lets assume the capacitor C1 is fully discharged first. At this state the output of U1A is HI, the G1 current source starts charging the capacitor C1. Once the voltage across this capacitor reaches the up threshold of U1A, G1 stops charging capacitor C1 therefore the this capacitor is being discharged with current source of G2, decreasing the voltage across this capacitor. When the voltage across the capacitor C1 reaches the lower threshold of U1A, the output of U1A turns on, causing the G1 start charging back the capacitor C1. This charging and discharging of capacitor C1 creates the output square waveform of the circuit, however, the frequency is determined by the amount of the current is provided by the current sources. Since the amount of this current is determined by input control voltage thus the output frequency of the circuit is determined by the value of input voltage. The output of the VCO is used to drive the MOSFET switch transistor of the Class-E coil-driver.

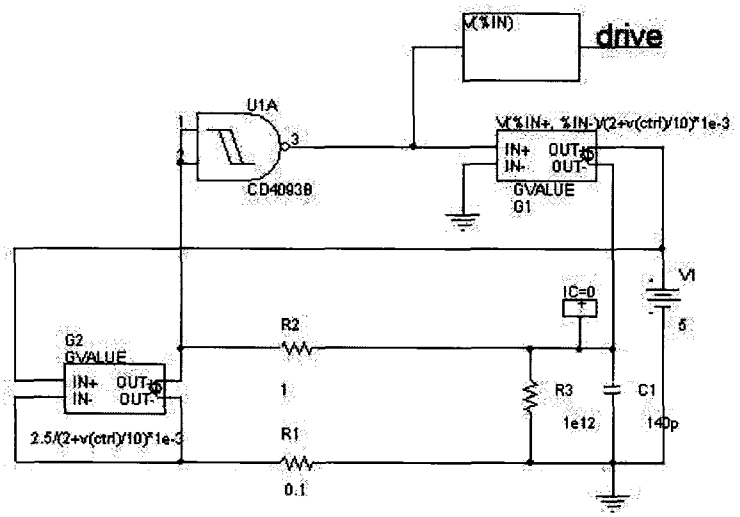

Figure 6.9 The behaviorial VCO in SPICE

Figure 6.10 shows the output of the proportional amplifier. The output of this amplifier, after being integrated by the integration amplifier, is shown in Figure 6.11.

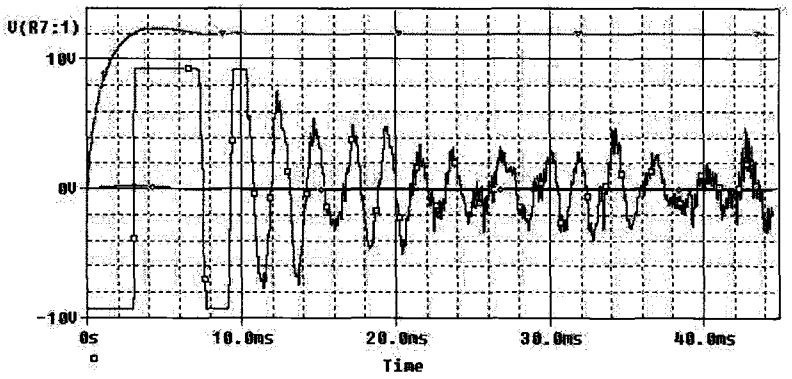

Figure 6.10 The output waveform of the proportional amplifier in the closed control loop

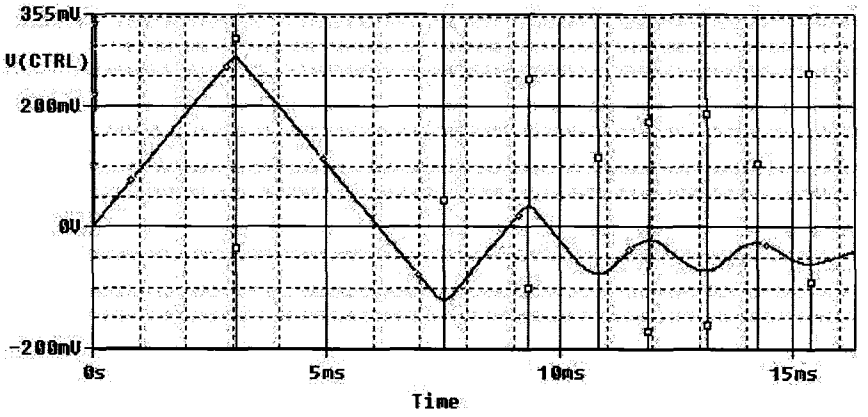

Figure 6.11 The output waveform of the integrator amplifier in the closed control loop

As can be seen the output of the difference amplifiers/compensator is reduced to 50 mv after a transient time of 15 ms. Figure 6.10 also include the output voltage of the system. As can be seen this voltage after a transient time of 10ms is stabilized while the its overshoot is limited to 2 v at its start up.

6.2 Experimental Results

After realization of the circuit, the output and drain voltage waveforms obtained from the experimental results are depicted in Figures 6.12 to 6.17. In this figures the waveforms in channel 1 and channel 2 correspond to drain and output voltages respectively. The Y axis represents the voltage whose resolution is mentioned underneath each figure for each corresponding channel and the X axis represents time whose resolution is mentioned at the top of each figure. One can see that there is a great resemblance between the simulation and the experimental results in terms of the interpretation of the waveforms. For example both of the simulation and the experimental waveforms' amplitude follow the frequency transfer function of the Figure 6.1 and the frequency band on which the safe operation could be maintained are very close to each other. The differences between the simulation and experimental waveforms, however, could be attributed to parasitics such as the equivalent series resistances and capacitances of the coils as well as the drain capacitance of the switch transistor. The experimental waveforms of Figures 6.12 to 6.17 indicate that in the frequency band of 392 kHz to 408 kHz, where the ZVS can be maintained, the output voltage can be controlled between 12.6 v to 9.8 v.

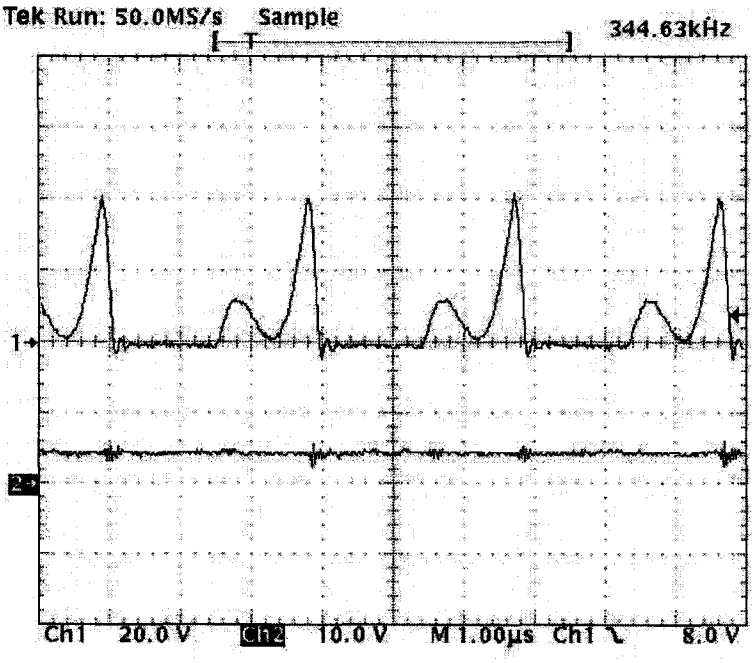

Figure 6.12 Experimental drain and output waveform at frequency of $f_{op} = 344$ kHz

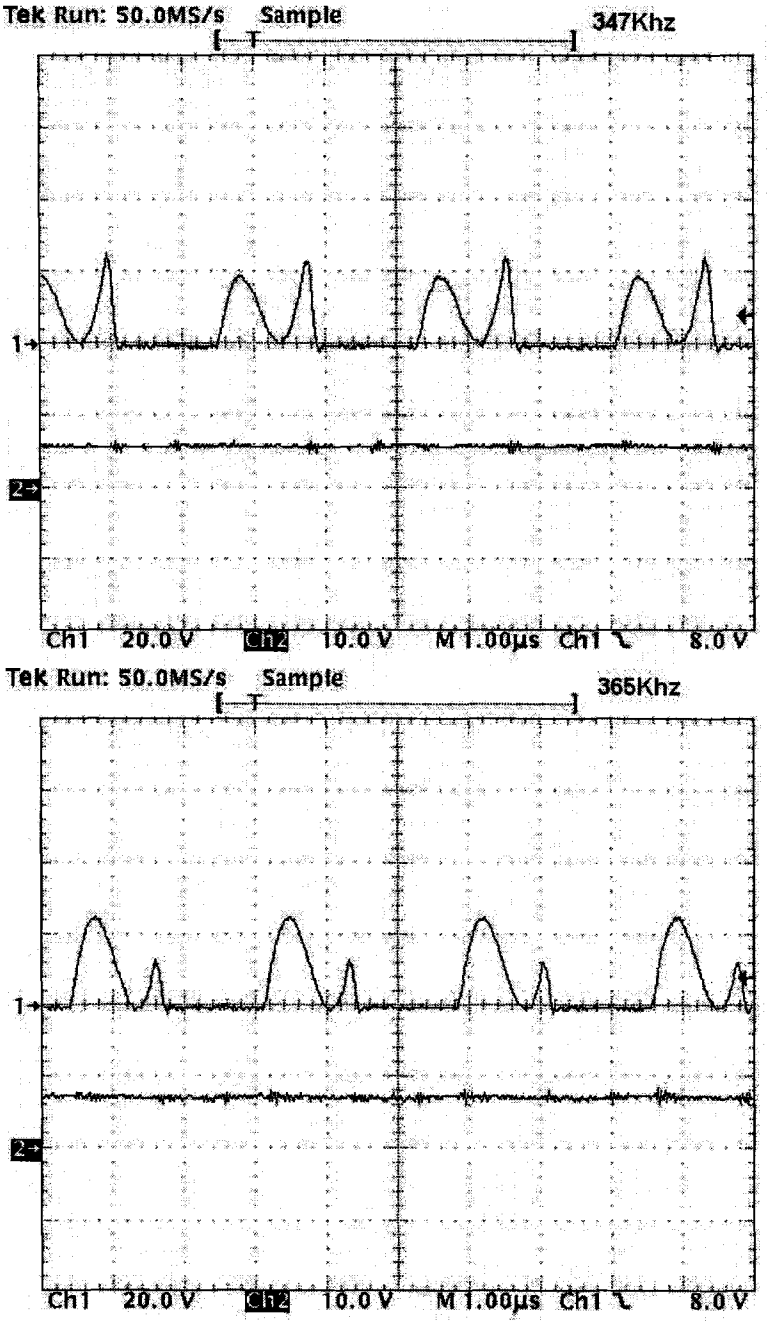

Figure 6.13 Experimental drain and output waveform at frequencies of $f_{op} = 347$ kHz and $f_{op} = 365$ kHz

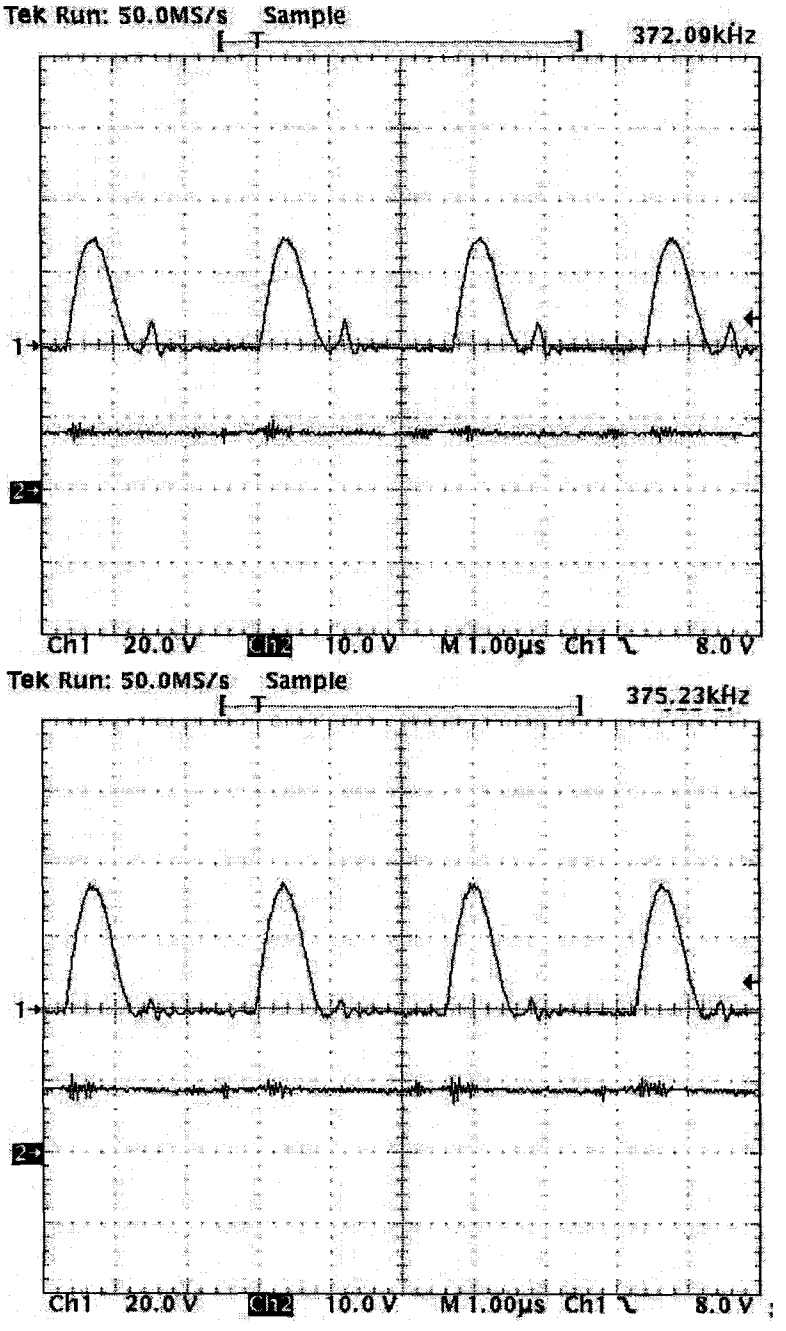

Figure 6.14 Experimental drain and output waveform at frequencies of $f_{op} = 372$ kHz and $f_{op} = 375$ kHz

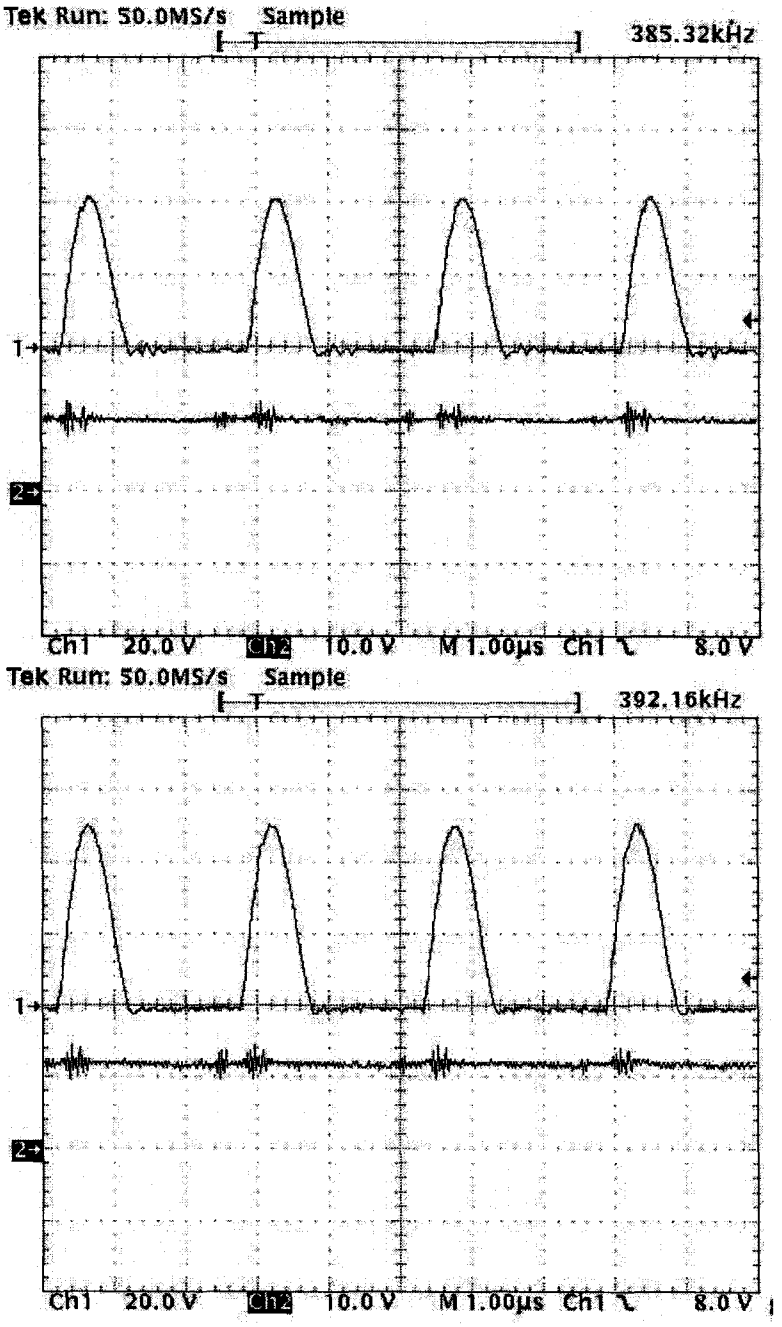

Figure 6.15 Experimental drain and output waveform at frequencies of $f_{op} = 385$ kHz and $f_{op} = 392$ kHz

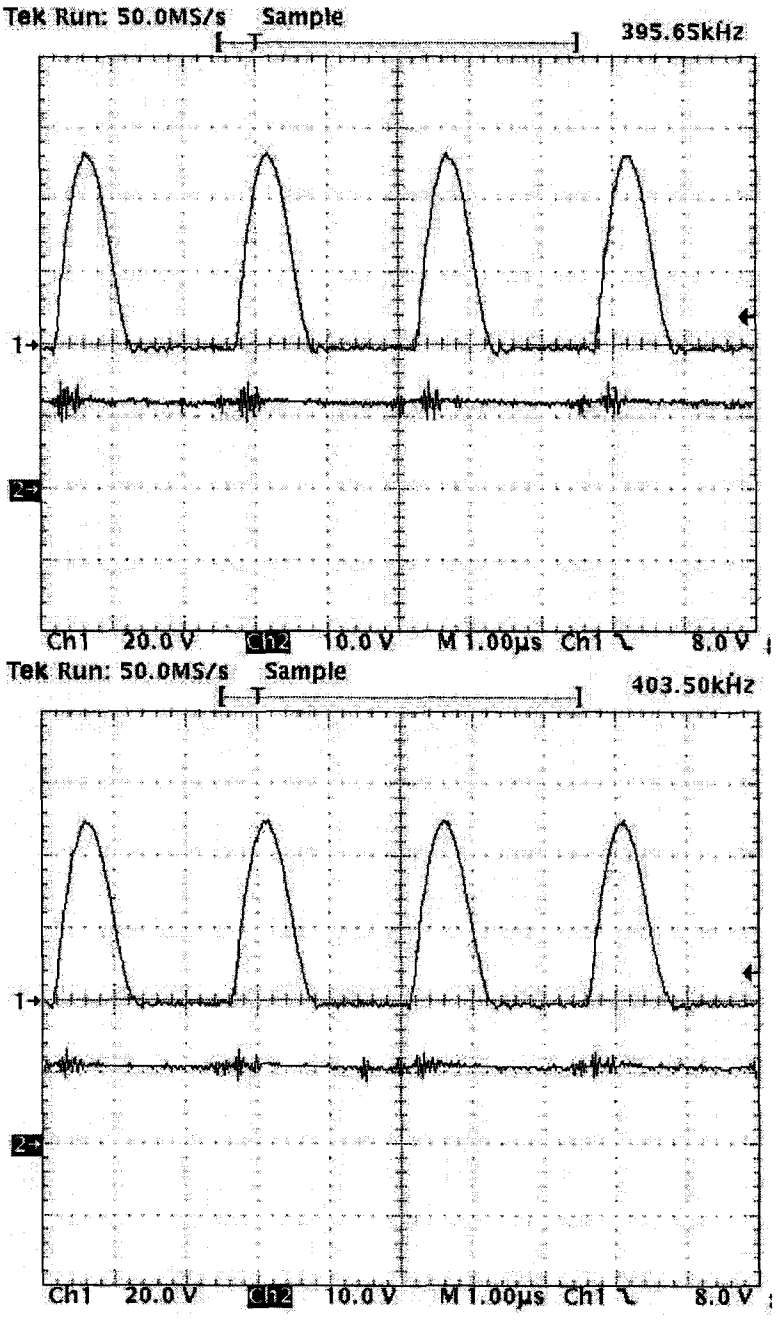

Figure 6.16 Experimental drain and output waveform at frequencies of $f_{op} = 395$ kHz and $f_{op} = 403$ kHz

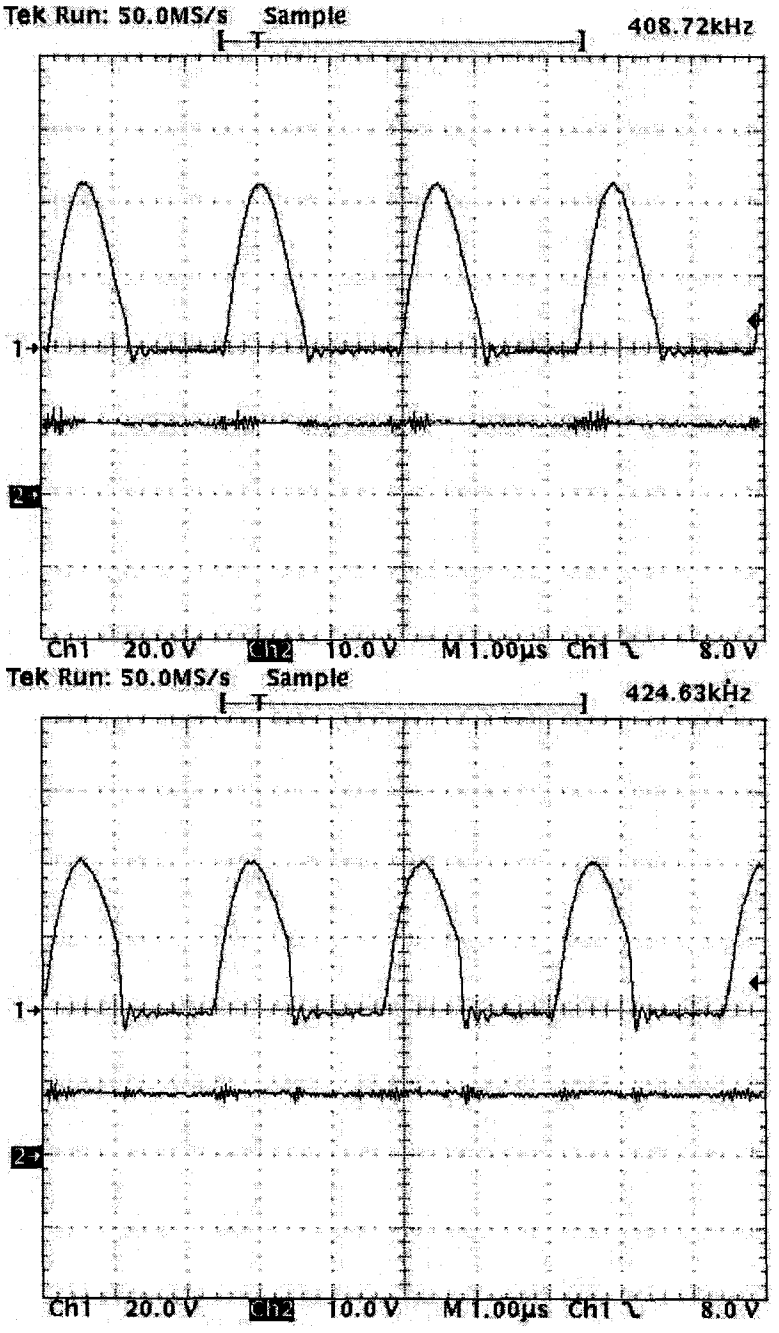

Figure 6.17 Experimental drain and output waveform at frequencies of $f_{op} = 408$ kHz and $f_{op} = 424$ kHz

To have a better insight of the performance of the designed transcutaneous energy transfer system, the efficiency graph of the system at different working conditions would be helpful. The efficiency here is defined as the ration of the output delivered power to the load to the input power delivered to the system. The efficiency versus operating frequency for three different coil separation distances (air gap) found from experimental results are shown in Figure 6.18.

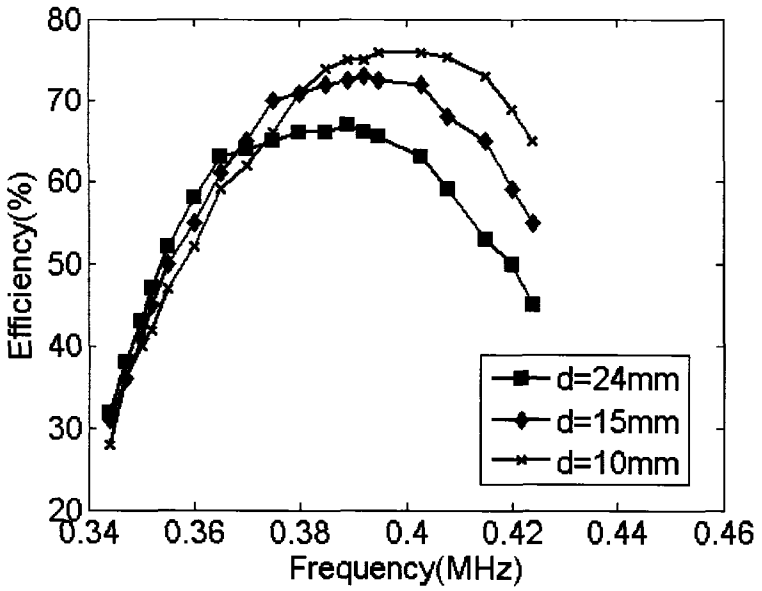

Figure 6.18 Efficiency versus operating frequency for different coils distances

The safe operating frequency band is defined here as the frequency band over which the zero voltage switching condition is maintained. This band is considered to be safe since beyond that not only the efficiency degrades bus also switching losses raises which may lead to the destruction of switching transistor in short term. It can be seen that the safe band for operating frequency of the system for the coils septation distance of 24mm is between 360 to 410 kHz. This band for separation distances of 15mm and 10mm are 370 and 410 kHz and 380 and 420 kHz respectively. This suggests that the frequency band of 380 and 410 kHz can be chosen for controlling

the output voltage of the system in spite of coils separation variation from 10mm to 24mm.

Depending on the application of the system it might be necessary to have the graphs pertaining to effects of lateral displacement of the coils on the output voltage as well. This performance is not as important as compared with the effect of separation displacement and doesn't have significant value when, in general, the main performance of the system is studied. In those application that the probability of lateral displacement would be significant, to stabilize the effect the system against it, the geometrical technique would be used as explained in Chapter 2. In this case the study of lateral displacement must be performed to evaluate the effectiveness of the method used.

6.2.1 The Prototype System

The pictures of the prototype system fabricated for experimental measurement are shown in Figures 6.20, 6.19, and 6.21.

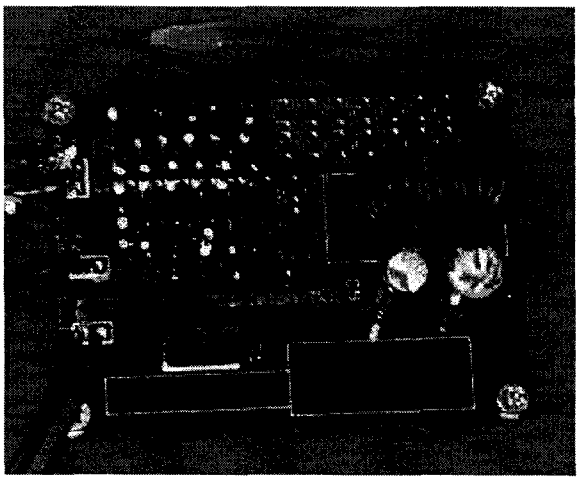

Figure 6.19 The implanted board of the Class-E frequency-controlled transcutaneous energy transfer system designed for this thesis (size = 4.5 x 6 cm^2)

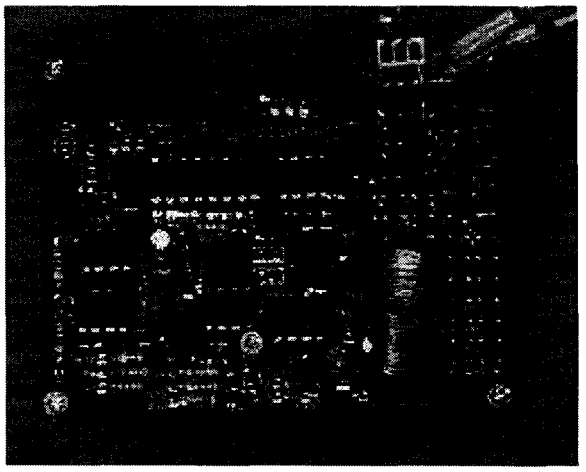

Figure 6.20 The External board of the Class-E frequency controlled transcutaneous energy transfer system designed for this thesis (size = 6.5x8 cm^2)

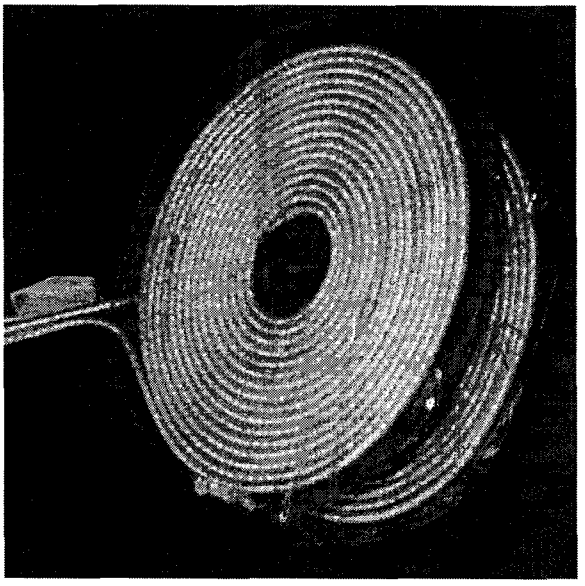

Figure 6.21 The transcutaneous transformer of the Class-E frequency controlled transcutaneous energy transfer system (diameter of each coil = 8 cm)

These board are designed just for experimental measurements to evaluate the modeling and design method of the target system. Many practical concerns were not the the main objective to achieve at this step. The feedback of the system is implemented by hard wire therefore the effects of the wireless or infra-red transcutaneous transceiver should be separately considered when those are implemented in the future work.

Other than the coils of the transcutaneous transformer, the coils L1 and L4 in Figure 6.22, are chosen from ordinary coils which easily are found in a switching power supply like a computer power supply. Using better quality and smaller coils will be considered in the next version of this work. The capacitors C1, C2, C3 and C4 must be very low ESR (equivalent series resistor) since all the transferred power are passing or swing though them. In this work a large number of ordinary polyester capacitors are paralleled to reduce the equivalent total resistance of them.

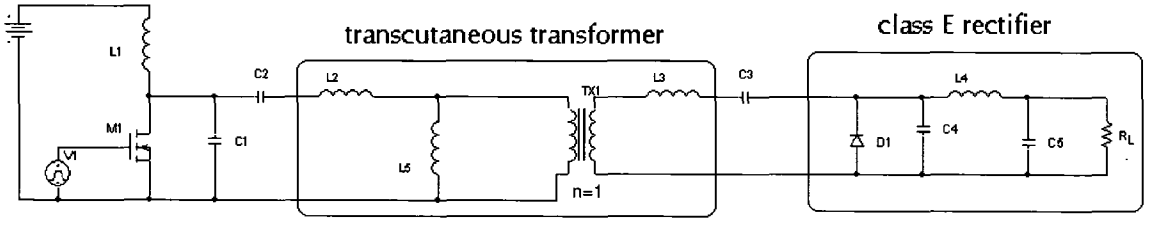

Figure 6.22 The schematic diagram of power transfer section of the proposed transcutaneous energy transfer system

The switching transistor here is IRF152 which can tolerate maximum voltage of 100 v and maximum current of 10 A. The on-state resistance of this transistor is 0.1. The output diode, D1, is a schottcky diode whose on-state voltage-drop is 0.4 v and can tolerate a reverse voltage of 40 v. Part of system losses are associated with the

on-state voltage drop of the output diode and the on-state resistance of switching transistor.

The rail voltages of the system are ±5 v which are created by a small switching power supply, which produces the +5 v, and a switch-capacitor system which inverts the +5 v to create a -5 v from it. These supplies are used to power up the op-amps, which are used to create the difference amplifier and the compensator circuit, as well as, supplying the VCO and the switching transistor driver of the circuit.

The operating frequency of this system is about 400 kHz. Although one might speculate that increasing the operating frequency would reduce the size of the transcutaneous coils, but in biomedical application to which this work would be used it is not true. Size of the transcutaneous coils are determined by so many factors such as coils wire resistance, working temperature constraint, the implantation place and required limit of efficacy for the system. Reducing the size of the coils by frequency is only allowed when all these requirements are satisfied.

Chapter 7

CONCLUSIONS, CONTRIBUTIONS AND FUTURE WORK

In this thesis a method for designing a transcutaneous energy transfer system is presented and based on that a system is designed, simulated, constructed and tested. This system uses a Class-E power amplifier for driving the primary coil of a transcutaneous transformer and also a Class-E rectifier at the secondary coil side, which is implanted. In this system the operation frequency variation is used to control the output voltage as well as to compensate the effects of the coils mutual position variations and the load variations on the output voltage. The simulations and experimental results indicate that this method for designing a transcutaneous energy transfer system is not only feasible but also a very promising method for controlling the output voltage and compensating the effects of coils mutual positions on the system. The closed-loop control system used to control and adjust the operation frequency provides a self-tuning capability for the system which does not require a complex circuitry with excessive component count. This self-tuning capability along

with the small component-count are the indication of small system size, more reliability and good efficiency of the proposed system.

7.1 Summary

In this thesis, after the introduction of a frequency-controlled Class-E transcutaneous energy transfer system, its operation analysis, design method and simulation and test results are reported. The analysis procedure for each block of the system is either illustrated or referred to their relevant references for more details, nevertheless the MATLAB programs for design and analysis of each subsection are written. These programs are used to mathematically model the system operation for analysis purposes and also are used like a CAD tool to design each section of the system throughout this work. These models were also optimized and debugged in the course of performing this thesis. The design of the power section was simulated by PSPICE whose results are used for starting the experimental phase of this work. A closed-loop analysis is performed using SIMULINK to determine the values of the components required for the compensation circuit.

Designing the transcutaneous transformer is a challenging work in this thesis. By finding the guidelines for winding the coils in the literature, first the initial design was simulated by HFSS to find the self and mutual inductances of the coils. After the optimization process at this step, the coils are wound and through practical procedure the self and mutual inductances are measured and determined and the results are compared to simulation results for verification and validation purpose.

Once the system is designed, its performance over the band of working frequencies,

suggested by analysis, is evaluated and accordingly the suitable particular operating band in which the safe and high performance operation are predicted is selected. A control circuitry is devised to control the output voltage by variation of the operating frequency. This control circuitry works on the principle that the result of the caparison of output voltage and a reference voltage is amplified and fed to a VCO whose output drives the switching MOSFET. The compensation circuitry whose design values are determined with analysis by SIMULINK is used to either integrate or differentiate the variation of the output voltage for the stability of the closed-loop and quick reaction to any changes of voltage due to load, input voltage or the coils separation distance changes.

7.2 Remarks

The simulations and experimental results indicate that the frequency-control method is very promising for controlling the output voltage of a Class-E transcutaneous energy transfer system. This control is necessary to compensate for the effects of coil misalignments, the effects of exposing a metal object to the coils and the load and input voltage variations. The experimental results confirm that this method is highly efficient, provided that the operating frequency of the system is adjusted at zero-voltage switching (ZVS)areas of the transfer function. The ZVS areas can be determined analytically or through simulations as outlined in Chapter 6.

The interaction of the secondary tuned filter with the Class-E coil driver provides more flexibility in choosing the desired frequency band for the system operation as well as choosing the desired control methodology according to the selected area of the

transfer function. This step of the design has a significant effect on the overall system performance. The optional selection of the relative positions of resonant frequencies of the Class-E coil-driver and the output tuned filter versus operation frequency provides flexibility in choosing the desired features for the transfer function for the system. Among these optional features are the linearity of the transfer function, either negative or positive slope of frequency versus output voltage control and the desired control frequency band.

One should be cautious about the parasitics in the real circuit and include them in circuit simulation to have the expected results in the practical tests. Parasitics that should be taken into account are the drain-source capacitance and ohmic resistance of the switch transistor as well as parasitic capacitance of the coils at the operating frequency and the equivalent series resistance (ESR) of the capacitors. It is extremely important to note that all the transferred power is passed through the series and parallel capacitors of the Class-E coil-driver and the Class-E rectifier. If these capacitors have large equivalent series resistances (ESR), the systems endures a great loss.

This method does not require a dc-dc converter at the front side as opposed to voltage controlled Class-E method which uses this converter to control the input voltage to adjust the current driven to the primary coil for the required output voltage. This method does not either require a complex circuitry for compound frequency and duty cycle control as opposed to frequency-tracking method and after all it employs Class-E coil-driver controlled by frequency as opposed to series resonant coil-driver controlled by frequency. The Class-E coil-driver is superior over series-resonant coil driver in terms of eliminating both turn-on and turn-off of the switching transistor of

the system.

Intrinsically, the frequency controlled Class-E coil-driver has a good consistency with the system for compensating for coil displacements. The coil displacements result in variation of leakage and coupling inductances which are incorporated into the structure of Class-E coil-driver. That is, when the problem is seen from the reverse side, when frequency varies, the series inductance of the Class-E coils driver must be varied too and one of the way that this may happen is by displacements of the coils. Of course there are some constraints as to what extent these variations are tolerable which is one of the challenges for a good design. This means that for a perfect design, according to this method, the limits of coils displacements should have already been defined and made sure those could be covered in the safe and low-loss operating points of the designed system. A design in which these aspects are already considered can be truly called a self-tuned design. The self-tuning capability along with the small component count of the introduced system are the indications that the system designed with this approach has small size, is reliable, and has good efficiency.

7.3 Contributions

The contributions have been made by this work are listed below.

- Controlling frequency of a Class-E coil-driver to keep the output voltage of a transcutaneous energy transfer system regulated
- Utilizing the combination of Class-E coil-driver and Class-E rectifier with a transcutaneous transformer
- Studying the effects of secondary tuned filter to eliminate the secondary leakage inductance and on overall system operation.

- Modeling the operation of frequency-controlled Class-E in MATLAB
- Modeling the transcutaneous coil-driver in HFSS for any type of cross-section for the winding wire and polygon turning loop instead of circular loop to maximize simulation speed
- Fabrication of a prototype Class-E frequency controlled transcutaneous energy transfer system which verifies the analysis and simulations

7.4 Future Work

There are a couple of things that will complete this work at the in-vitro level. The first thing is adding a wire-less transcutaneous transceiver to the system and to do all the stability analysis with the effects of the new parameters introduced to the system.

Trying to raise the efficiency of the system while reducing the size of the implanted circuit would be the other objective. There are so many practical issues that should be solved in the preparation course of the system before starting the in-vivo tests. Preventing the effects of the electromagnetic filed on the circuits, specially the implanted one, and its physical situation with respect ot the implanted coil is one of them. Using high quality coils for the Class-E rectifier system and the input of the Class-E amplifier and replacing the current parts with surface-mount part and using multi-layer PCB to reduce the effect of noise and electromagnetic filed on the system should also be considered in this step.

This work has demonstrated great promises for employing the Class-E frequency controlled transcutaneous energy transfer system, however, to have a clear view of the merits of this system over the previous ones, designing the prototypes of the previous

systems for the same application would be suggested.

Designing a CAD system specific for designing frequency-controlled transcutaneous energy transfer system which can utilize all the MATLAB programs written during this research would be another idea. Most of the design considerations, remarks and iterations could be included in the prospect CAD which could ensure all the details are considered into the design.

Applying the same approach for designing transcutaneous energy transfer system for applications with different specifications and requirements would certainly help to find problems were not seen at this work and make the method more comprehensive.

References

1. G. Wang et. al., "A Closed Loop Transcutaneous Power Transfer System for Implantable Devices with Enhanced Stability," *Proceedings of the 2004 International Symposium on Circuits and Systems, ISCAS*, Vol. 4, pp. 17-20, May 2004.

2. A. Ghahari and Bo. H. Cho, "Design of a Transcutaneous Energy Transmission System Using a Series Resonant Converter," *IEEE Transactions on power Electronics*, Vol. 7, No. 2, pp. 261-267, Apr. 1992.

3. R. Puers and G. Vandevorde, "Recent Progress on Transcutaneous Energy Transfer for Total Artificial Heart Systems", *Artificial Organs*, Vol. 25, No.5, pp. 400-405, May. 2001.

4. G. B. Joung and Bo. H. Cho, "An Energy Transmission System for an Artificial Heart Using Leakage Inductance Compensation of Transcutaneous Transformer," *IEEE Transaction on Power Electronics*, Vol. 13, No.6, pp. 1013-1022, Nov. 1998

5. J. A. Miller, G. Belanger and T. Mussivand, "Development of an Autotuned Transcutaneous Energy Transfer System," *ASAIO*, Vol. 39, pp. M706-M710.

6. J. C. Schuder, "Powering an Artificial Heart: Birth of the Inductively coupled-Radio frequency system in 1960", *International Society of Artificial Organs, Blackwell Publishing Inc.*, Vol. 26, No. 11, pp. 909-915, 2002.

7. T. Mussivand, A. Hum and K. S. Holms, " Remote Energy Transmission for Powering Artificial Hearts and Assist Devices," *Cardiovascular devices, University of Ottawa Heart Institute,* Ontario, p344-347.

8. M. Soma et. al., "Radio-Frequency Coils in Implantable Devices: Misalignment Analysis and Design Procedure," *IEEE Transactions on Biomedical Eng.,* Vol. BME-34, No. 4, pp. 276-282, Apr. 1987.

9. C.M. Zienhofer and E. S. Hochmair, "Geometric Approach for Coupling Enhancement of Magnetically Coupled Coils," *IEEE Transactions on Biomedical Eng.,* Vol. 43, No. 7, pp. 708-718, Jul. 1996.

10. E. S. Hochmair, "System Optimization for Improved Accuracy in Transcutaneous Signal and Power Transmission", *IEEE Transaction on Biomedical Eng.,* Vol 31, No. 2, pp. 177-86, Feb. 1984.

11. G. C. Galbrith and M. Soma, "A Wide-Band Efficient Inductive Transdermal Power and Data Link with Coupling Insensitive Gaib," *IEEE Transaction on BiomedicalEng.,* Vol. BME-34, N0. 4, pp. 265-275, Apr. 1987

12. C. M. Eierhofer and E. S. Hochmair, " High-Efficiency coupling-Insensitive Transcutaneous Power and Data Transmission via Inductive Link", *IEEE Transaction on Biomedical Eng.,* Vol. 37, No. 7, pp. 716-722, Jul. 1990.

13. M.C Zierhofer and E.S. Hochmair, "Transcutaneous transmission of Digital Data and Energy in a Cochlear Prosthesis System", *The International Journal of Artifivial Organs,* Vol. 15, No. 6, pp. 378-382, 1992.

14. C. G. Kim and Bo. H. Cho, "Transcutaneous Energy Transmission with Double Tuned Duty Cycle Control," *IECEC 96, Proceedings of the 31st Intersociety,* Vol. 1, pp. 587 - 591, Aug. 1996.

15. T. H. Nishimura et. al., "An Improvement of a Transcutaneous Transformer for a Non Invasive Recgargeable Cardiac Pacemaker Battery," *PESC '96 Record., 27th Annual IEEE,* Vol. 1, pp. 316 - 321, Jun. 1996.

16. N. O. Sokal and A. D. Sokal, "Class E - a New Class of High-Hfficiency Tuned Single-Ended Switching Power Amplifiers," *IEEE Journal of Solid-State circuits,* Vol. 10, No. 3, pp. 168-176, Jun. 1975.

17. P. R. Troyk and M. A. K. Schwan "Closed-Loop Class-E Transcutaneous Power and Data Link for Micro-Implants," *IEEE transactin Biomedical Eng.,* Vol. 39, No. 6, pp. 589-599, Jun. 1992

18. G. Wang et. al., "Design and Analysis of an Adaptive Transcutaneous Power Telemetry for Biomedical Implants," *IEEE Transaction on Circuit and System,* Vol. 52, No. 10, pp. 2109 - 2117, Oct. 2005.

19. *Power Electronics course note, Colorado University,* http: ece-www.colorado.edu/ ecen5797/notes.html

20. R. Steigerwald, "A Comparison of Half-Bridge Resonant Converter Topologies," *IEEE Transaction on Power Electronics,* Vol3, No.2 , pp. 174-182, Apr. 1988.

21. S. Atluri and M. Ghavanloo, "Design of a Wideband Power-Efficient Inductive Wireless Link for Implantable Biomedical Devices Using Multiple Carriers," *Proccedings of second International Conference of IEEE EMBS on Neural Eng., Arlington, Virginia,* pp. 533-537, March 16-19 2005.

22. M. K. Kazimerczuk and K. Puczko, "Exact Analysis of Class E Tuned Power Amplifier at Any Switch Duty Cycle," *IEEE Transactions on Circuits and System,* Vol. 34, No. 2, pp. 149-159, Feb. 1987

23. F. H. Raab, "Idealized Operation of the Class E Tuned Power Amplifier," *IEEE Transactions on Circuits and System,* Vol. 24, No. 12, pp.725-735, Dec. 1977.

24. H. Matsuki et. al., "Flexible Transcutaneous Transformer for Artificial Heart System," *IEEE Transactions on Magnetic,* Vol. 26, No. 5, pp. 1548-1550, Sept. 1990.

25. T. H. Nishimura et. al., "An Advanced Transcutaneous Energy Transformer for a Rechargeable Cardiac Pacemaker Battery by Using a Resonant DC to DC converter," *Proceedings of the 1996 IEEE IECON 22nd International Conference on Digital Object Identifier,* Vol. 1, pp. 524 - 529, Aug. 1996.

26. L. Zhao et. al., "Tanscutaneous Transformer in Power supply system for an Artificial Heart," *Power Electronic Drives and Energy Systems for Industrial Growth, International Conference on Digital Object Identifier,* Vol 1, pp. 348 - 352, Dec. 1998.

27. J. A. Blanchard and J. S. Yuan, "Effect of Collector Current Exponential Delay on Power Efficiency for Class E Tuned Power Amplifier," *IEEE Transactions on Circuits and System,* Vol. 41, No. 1, pp. 69-72, Jan. 1994

28. N. O. Sokal, "Class E high efficiency Power Amplifiers from HF to Microwave," *Proceedings of the IEEE international Microwave Symposium, Baltimore,* Vol. 2, pp. 1109-1112, Jun. 1998.

29. J. Rogers, C. Plett, *Radio Frequency Integrated Circuit Design* Artech House Inc., 2003

30. M. K. Kazimerczuk, "Analysis of Class-E Zero-Voltage-Switching Rectifier," *IEEE Transactions on Circuit and Systems,* Vol. 37, No. 6, pp. 747-755, Jun. 1990